UNIVERSITY OF CALIFORNIA

Los Angeles

Strain analysis for AlN thin-films on Si using high-resolution X-ray diffraction

A thesis submitted in partial satisfaction
of the requirements for the degree of Master of Science
in Materials Science and Engineering

by

Hrithik Agrawal

2024

ABSTRACT OF THE THESIS

Strain Analysis for AlN thin-films on Si
using high-resolution X-ray diffraction

by

Hrithik Agrawal

Master of Science in Materials Science and Engineering
University of California, Los Angeles, 2024
Professor Mark S. Goorsky, Chair

Aluminium Nitride (AlN) thin-films have been long used as a buffer layer on substrates to grow Gallium Nitride (GaN) for high power transistors. Researchers recently have started studying using AlN itself as an electronic material due to its higher band gap compared to GaN and applications in UV light source for photolithography systems. One of the main challenges of growing AlN on traditional substrates like Silicon (Si) is the large lattice mismatch and difference in crystal structures. Both these effects lead to strained and lower quality thin-films.

This study discusses the procedure for performing high-resolution X-ray diffraction (HRXRD) measurements, discussing equipment setup and choosing the diffraction peaks that are most suitable for this analysis. Symmetric and asymmetric scans were performed to calculate out-of-plane and in-plane strains respectively. Analysis of the full-width at half-maximum (FWHM) was done to qualitatively compare the film-quality for different samples.

This study analyzes the strain and film quality for AlN thin-films grown on Si. Two sets of samples have been analyzed – one with AlN thin-films grown on bare Si and second with a GaN nanowire interlayer between AlN and Si. The GaN nanowire layer serves to reduce the strain present in AlN by lowering the lattice mismatch compared to Si. All measurements have been performed using (HRXRD). Results show that samples with GaN interlayer have an almost completely relaxed AlN layer with better film quality compared to those grown on bare Si. The strain ranges from 0% to 0.3% for samples with GaN interlayer while AlN on bare Si sample has a strain of about 1%. For samples with the GaN layer, different thicknesses have been analyzed. Results indicate that the thicker layers are more strained and have a lower film quality. AlN films grown on bare Si were characterized for surface roughness and thickness using X-ray reflectivity (XRR). Data shows that the surface has a roughness of about 3 nm with the films being 200 nm thick. The presence of a GaN nanowire interlayer has shown to improve the AlN thin-films grown on Si, further paving the way for this material to be used in electronic applications.

The thesis of Hrithik Agrawal is approved.

Alexander A. Balandin

Aaswath P. Raman

Mark S. Goorsky, Committee Chair

University of California, Los Angeles

2024

Table of Contents

List of Figures

List of Tables

ACKNOWLEDGEMENTS

I would like to start by thanking my committee chair and advisor, Prof. Mark Goorsky. He has been instrumental in my learning throughout this project, both professionally and personally. Prof. Goorsky's teachings have been instrumental in my work as a master's student in the group. His focus on the finer details and knowing what you speak about are skills I wish to keep with me throughout my life.

A huge thanks to the entire Electronic Materials Group for their constant support. The entire group has been critical in the completion of this work. Without their support, completing this project would have been unimaginable. Everything I know about XRD and a lot that I know about life has come from discussions with my fellow colleagues and I am forever grateful for that. Special thanks to Brandon Carson for giving me an invaluable intuition to understand diffraction and being patient with my relentless and sometimes repetitive questions.

To my friends who have stuck around, I am grateful for all the companionship and support I have received. There are a lot of people to name who have backed me in my times of need. I am thankful beyond words for the moral support I have received.

Lastly, none of this would have been possible without the unconditional support from my parents. My parents and my sister are the reason I am able to take on challenges in life, knowing I have people to fall back on. I hope to emulate their teachings and make them proud through my work.

1 INTRODUCTION

Aluminium Nitride (AlN) has emerged as an important material in recent times. AlN is an ultra-wide bandgap material with a bandgap of around 6.2 eV. An important feature of AlN is that it is a direct bandgap semiconductor meaning that it can be used in photonic applications with wavelengths corresponding to about 200 nm. This wavelength corresponds to the UV region, which makes AlN an excellent UV light source for applications such as photolithography.

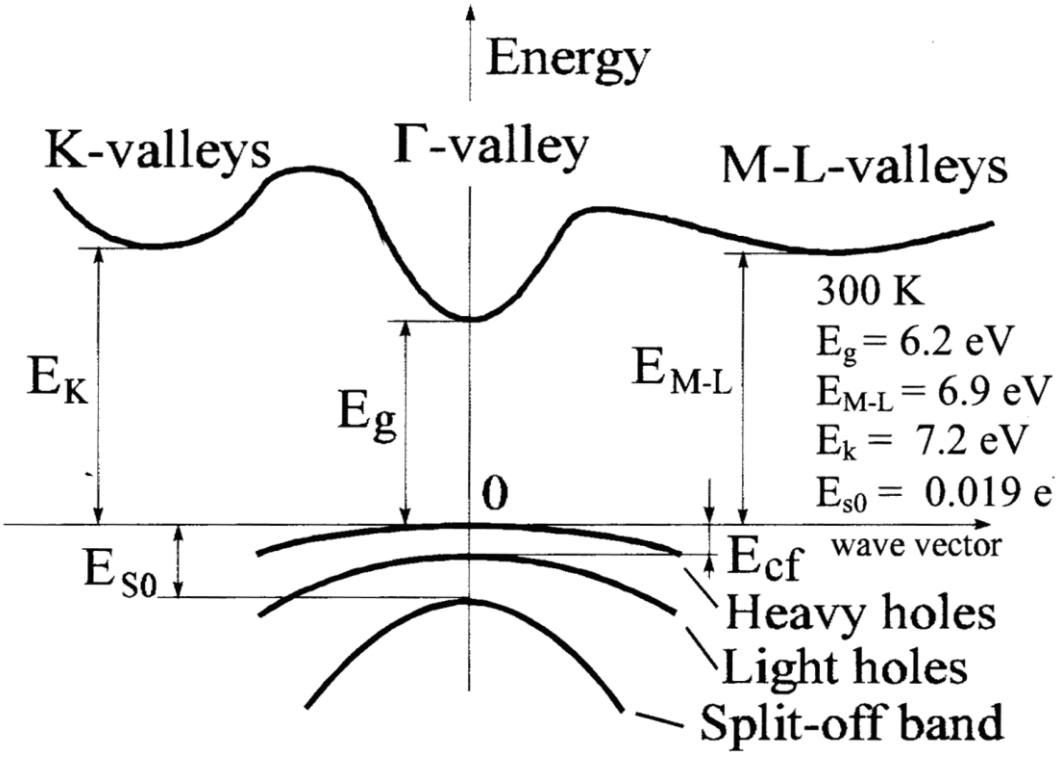

Figure 1: Band structure of wurtzite AlN [1]

AlN has a wurtzite hexagonal structure with in-plane lattice parameter (a) = 3.11 Å and out-of-plane lattice parameter (c) = 4.98 Å [2]. Due to its lattice parameter closely matching that of GaN, researchers have worked on using AlN as a buffer layer for the growth of GaN on substrates like Silicon (Si) and Sapphire (Al_2O_3) [3]. Studies conducted initially compared the

thickness of the AlN buffer layer and its effect on the structural and electronic properties of GaN deposited on top. Studies showed that having a higher buffer layer thickness lowered the strain in the epi layer [4]. Most studies involved characterizing AlN just for its effect on the epi-layer and not utilizing the properties of AlN itself. As deposition and growth techniques improved, more interest was given to growing better-quality AlN thin-films.

Substrates initially chosen for AlN thin-films were structurally similar materials such as Sapphire (Al_2O_3) [5] and Silicon Carbide (SiC) [6]. However, Si has emerged as the choice substrate for AlN for various reasons. First, Si is much cheaper compared to sapphire or silicon carbide. Second, growing high-quality Si is much easier resulting in larger diameter wafers. This makes the manufacturing of devices on these wafers more economical. These qualities make Si the preferred substrate for AlN thin-films. Researchers have long studied the optimal substrates for AlN. Most of the commonly used substrates have a very large lattice mismatch for AlN (except SiC). However, lattice mismatch is not necessarily the primary consideration when choosing a substrate. As demonstrated in fig. 2, Si and Quartz emerge as the substrates with the lowest roughness and smallest Full-Width at Half Maximum (FWHM) for AlN films deposited on them using reactive sputtering. Both Si and Quartz can be made into very smooth substrates, free of surface defects which grows high-quality AlN films. The FWHM has been compared for the (0002) hexagonal basal plane of AlN. This is done because the AlN thin-films are grown c-axis oriented. FWHM in a rocking curve can be used to understand the quality of the thin-film grown. The lower the value, the better quality the film is. Rocking curves are explained in detail in a later section.

As shown in fig. 2, Si can be used to grow very high-quality smooth AlN thin-films. However, the problem of a very large lattice parameter difference still remains. The lattice

mismatch between AlN and Si is about 42.7%. Such a high lattice mismatch makes the growth of defect-free thin-films very difficult.

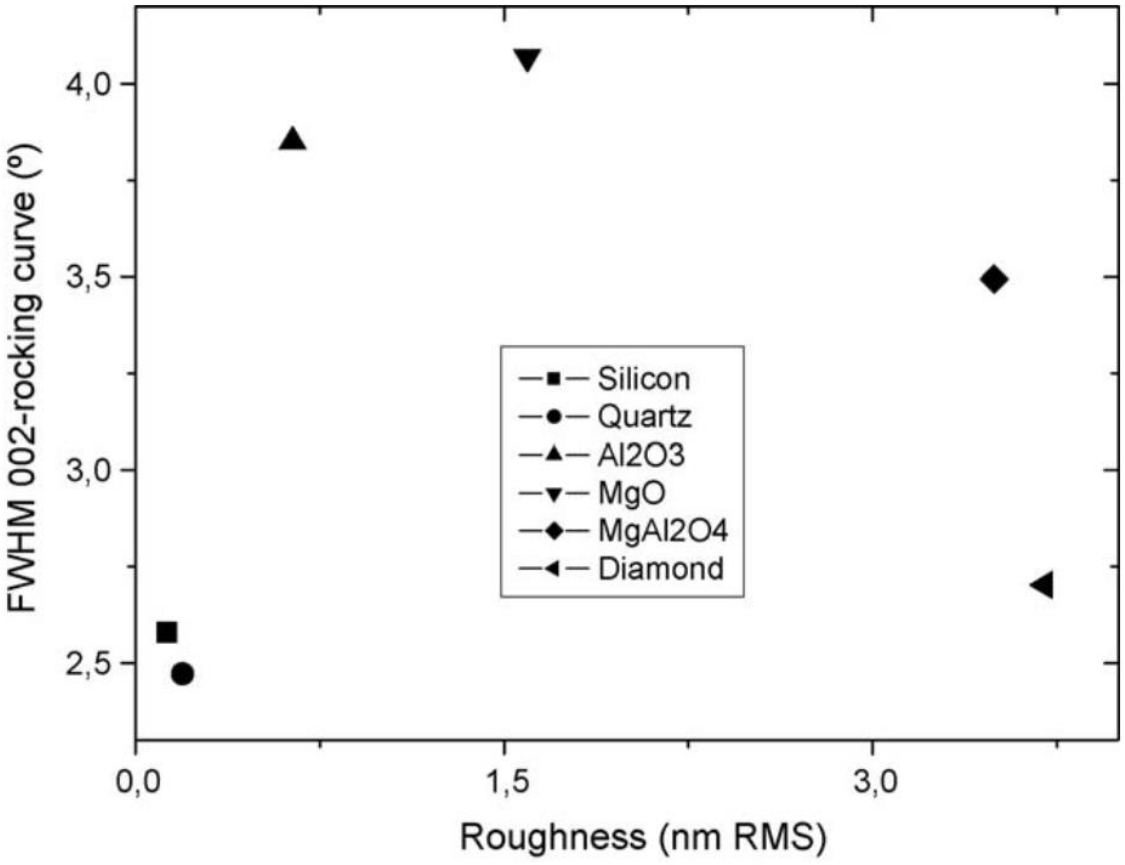

Figure 2: FWHM and roughness comparison for various substrates with AlN films deposited using reactive sputtering [7]

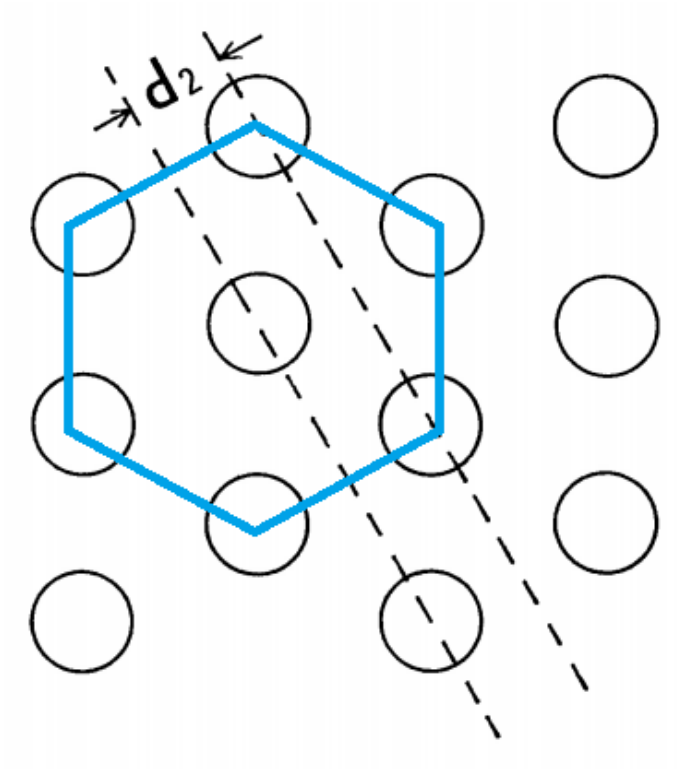

Figure 3: Atomic arrangement for Si as viewed from the (111) crystallographic direction [8]

As seen from fig. 3, the (111) atomic arrangement forms a pseudo-hexagonal structure, which helps in two ways. First, it becomes more structurally similar to the basal hexagonal plane for AlN. Second, the effective lattice parameter ($2d_2$ in fig. 3) becomes 3.84 Å [8]. The lattice mismatch now comes down to 19.01% from 42.7% for the (001) orientation. This lower lattice mismatch makes depositing high-quality AlN thin films with lower defects easier.

In this study, AlN thin films grown on Si (111) substrates with a GaN nanowire buffer layer are compared to structures consisting of just AlN on Si.. The schematic for the same is shown in fig. 4. The reason for introducing these nanowires is to further compensate the lattice mismatch and reduce the strain in the AlN films [3]. GaN has a lattice parameter of about 3.19 Å which means a lattice mismatch of about 16.93%. The AlN grown on top of the nanowire layer closely matches the lattice parameter with GaN and is, therefore, lower in strain. The

nanowires also serve as sites for nucleation. Most defects that occur are present near the coalescence boundaries, while the rest of the film is reported to have lower defect densities [3]. The key to this approach lies in growing high-quality GaN nanowires and ensuring that the defects are localized to the coalescence boundaries.

The samples have been grown using Molecular Beam Epitaxy (MBE) technique; further details can be found in the experiments section of the thesis.

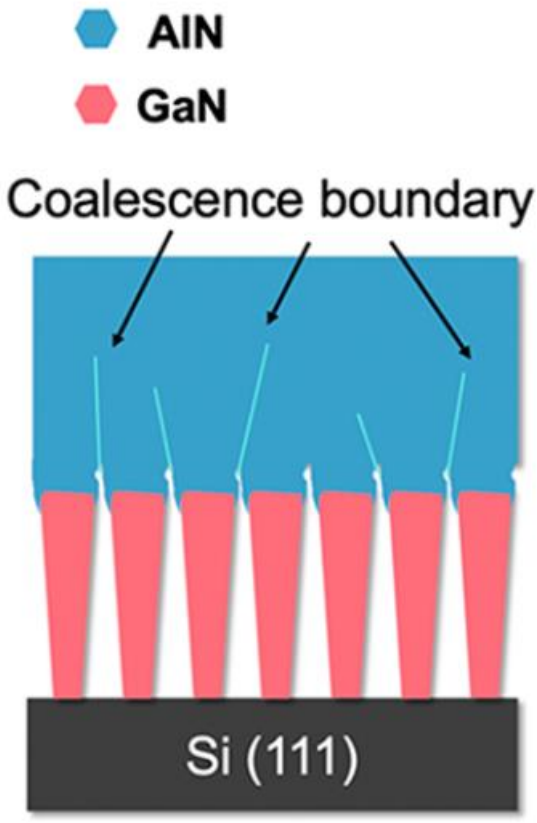

Figure 4: Schematic for AlN on Si (111) with GaN nanowire buffer layer grown using MBE [3]

2 BACKGROUND AND THEORY

2.1 X-Ray Diffraction (XRD)

X-Ray Diffraction (XRD) is a non-destructive technique used to analyse crystals. It is particularly useful for analyzing the crystallographic structure of materials. XRD is a powerful technique that can be used to identify phases and composition, calculate strains in thin-films, figure out the materials present, and much more. With in-situ measurements also easily done using XRD, this technique has found its application as a very reliable source of characterization in various fields of materials science.

The basic principle behind XRD is the interference of waves. The fundamental idea is that in-phase waves add in intensity while out-of-phase waves diminish. To be in phase, the waves must have a phase difference equal to an integer multiple of their wavelength. Out-of-phase interference has a phase difference of half-integer wavelengths. Diffraction will occur only at certain angles when the X-ray beam hits the sample. The intensity will be zero at all other angles because of destructive interference. This is depicted in fig. 5, where a beam of parallel x-rays hits a sample with atoms arranged as shown. The incident beam is “reflected” off the plane of atoms, and intensity is measured by a detector. In reality, the beam is not reflected off the atoms; instead scattering takes place and intensity is observed for the same angle as incidence. The incident beam is parallel, which is an important consideration for XRD. If the incoming is not parallel (divergent), there will be errors in the measurement.

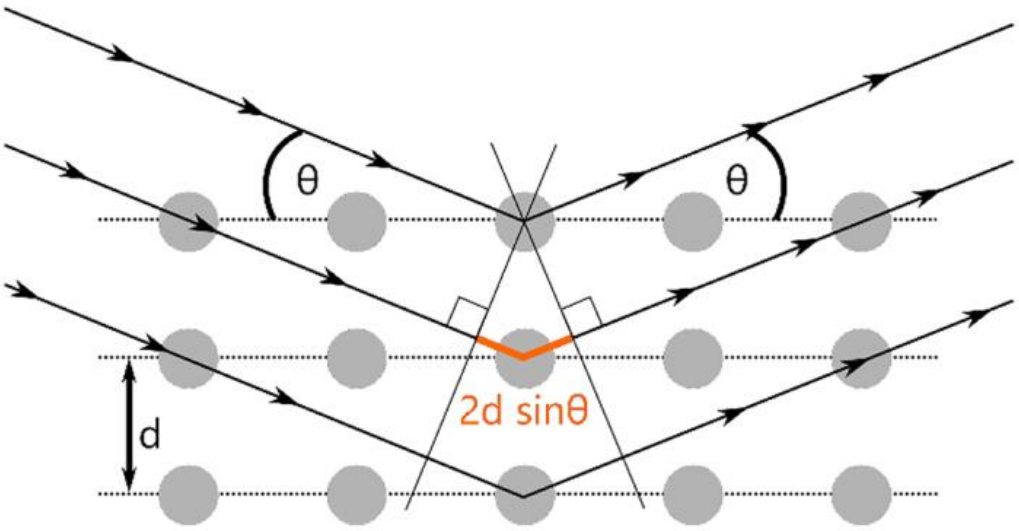

Figure 5: Diffraction from a plane of atoms by an incoming parallel x-ray beam [9]

Fig. 5 shows a parallel beam of X-rays hitting the sample at an incidence angle of θ. The beam is reflected back at the same angle, but different planes of atoms have different path lengths. The difference in the path length between two adjacent rows of atoms is equal to 2dsin(θ). Here, d is the distance between the adjacent plane of atoms. As discussed earlier in the section, for constructive interference to take place, the path length should be an integral multiple of the wavelength. This can be summarised using Bragg's Law given below.

$$n\lambda = 2d \sin\theta \tag{1}$$

Where,

n = order of diffraction (integer)

λ = wavelength of the X-ray used

d = interplanar distance

θ = Bragg angle for a particular plane

From Bragg's law, the angle at which intensity is observed (constructive interference) depends on the interplanar distance of the material. This quantity is dependent on the material's lattice parameter (a) and the plane being observed. The planes are referred using Miller Indices (hkl) for cubic systems and using Miller-Bravais Indices (hkil) for hexagonal systems. The equations relating lattice parameters to plane indices for hexagonal and cubic systems are given below.

$$d = \frac{a}{\sqrt{h^2 + k^2 + l^2}} \ (Cubic) \tag{2}$$

$$\frac{1}{d^2} = \frac{4}{3}\left(\frac{h^2 + hk + k^2}{a^2}\right) + \frac{l^2}{c^2} \ (Hexagonal) \tag{3}$$

Where,

d = interplanar distance

a = lattice parameter

h,k,l = Miller indices

For hexagonal lattices with four indices, the third index (i) is ignored because it is linearly dependent on h and k and is used only for geometric convenience.

2.2 Equipment Setup

A schematic diagram of the equipment used can be seen in fig. 6 below. It depicts the incident ray coming from the X-ray tube, which then hits the sample and reflects back on the detector. The angle between the incoming x-ray beam and the sample is labeled as ω and the angle between the X-ray beam and detector is labeled as 2θ. This is because the angle is twice the Bragg angle for a particular reflection. The angle 2θ is measured but all calculations require θ in them.

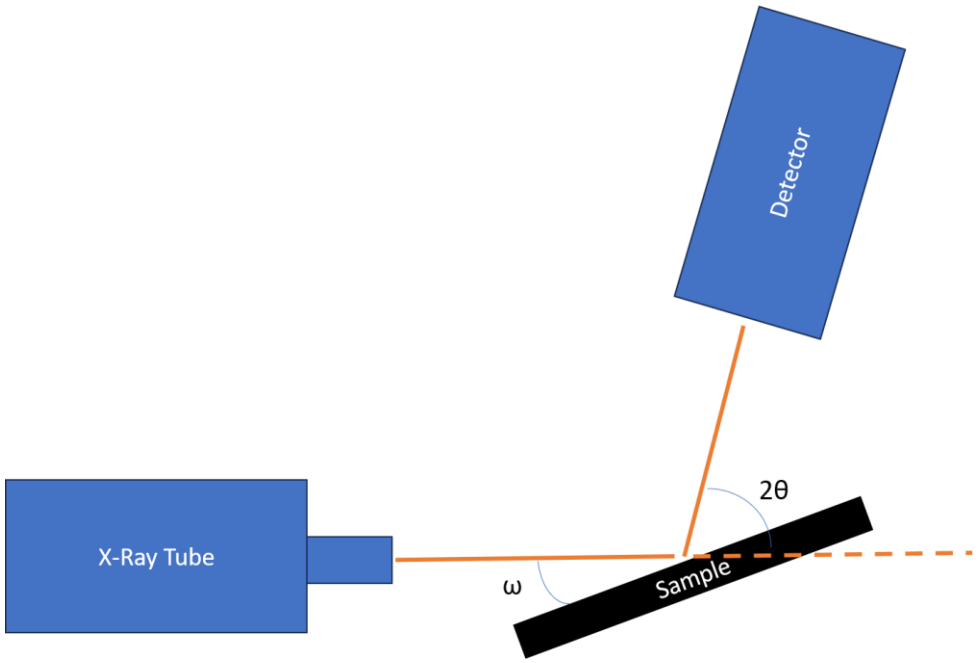

Figure 6: Top down view schematic for the X-ray diffraction equipment used

In the equipment used, the sample rotates to control ω while the detector moves to control 2θ. Along with ω and 2θ, there are a couple of other rotations that are available for the sample. These are namely chi (χ) and phi (φ). These rotations are depicted in fig. 7.

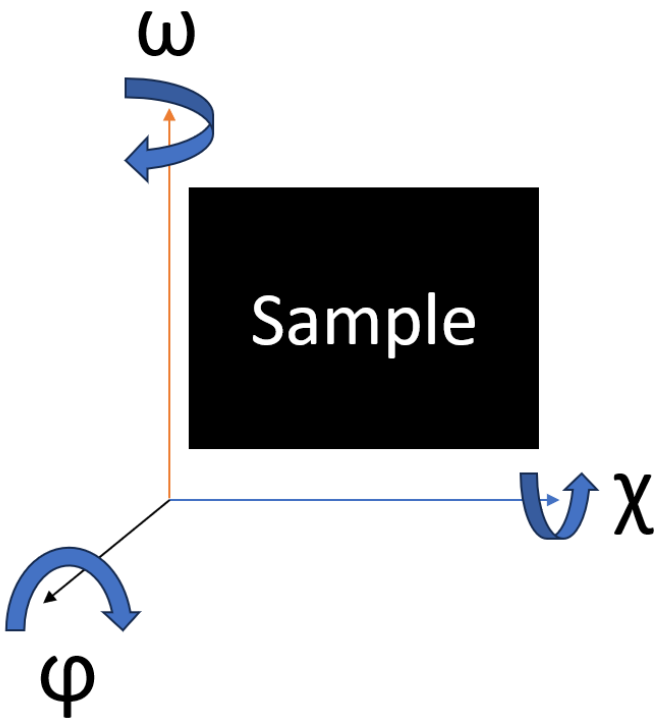

Figure 7: Schematic for chi and phi rotations of the sample corresponding to out-of-plane and in-plane rotations respectively

All of these independent controls on the XRD tool help observe relevant crystallographic peaks for various materials. Broadly, the peaks can be categorized into two: symmetric and asymmetric. Symmetric peaks are planes that are oriented in the same direction as the surface. For example, if the surface is (111) oriented, the planes (222), (333), etc. will be symmetric planes. For these planes, $\omega = \theta$, which means that ω and 2θ motors move in a ratio of 1:2 (also known as ω:2θ scans or θ:2θ scans). All other planes that are not parallel to the surface plane are known as asymmetric planes. For example, the (133) plane for a (111) surface-oriented material will be asymmetric. For these planes, ω and 2θ are not in a 1:2 ratio,

there is another component that comes from the interplanar angle between the desired reflection and surface orientation. The relationship between ω and θ is given by the equations below.

$$\omega = \begin{cases} \theta - \phi & for\ G.I \\ \\ \theta + \phi & for\ G.E \end{cases} \tag{4}$$

Where,

θ = Bragg Angle for the desired reflection

ϕ = Angle between the surface plane and desired reflection

G.I = Glancing incidence

G.E = Glancing exit

The only difference between G.I and G.E conditions is the angle at which the incoming X-ray beam strikes the sample and gets reflected. For G.I scans, the incidence angle is very small, but the reflected beam is very broad. For G.E. scans, the incidence angle is large, but the reflected beam is narrow and at a glancing angle to the sample. For this reason, G.E. scans are chosen since they have a better resolution. This phenomenon is depicted in fig. 8.

To analyze the strain in a sample, lattice parameters are calculated and then compared to the reference values. This involves an extra step for hexagonal materials since two lattice parameters are involved for some reflections, a (basal) and c (vertical). Using eqn. 3, a and c

can be calculated if two different non-parallel (asymmetric) reflections are known with their interplanar spacing known from Bragg's law. Another approach to this is to separate the a and c lattice parameter terms in eqn. 4 by choosing a plane of type (000l) which only has the c part. Then by choosing any other plane, a lattice parameter can be calculated independently. Since AlN is (0001) oriented, the (0002) plane can be observed for "c" and then choose an asymmetric scan to calculate the "a" lattice parameter. Mapping out the crystallographic peaks has been discussed further in the section.

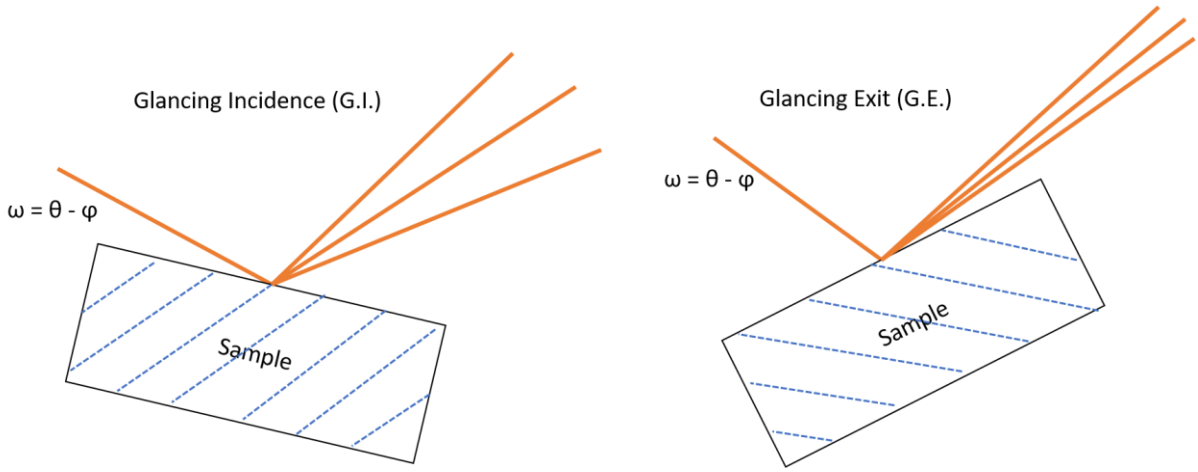

Figure 8: Schematic for Glancing Incidence (G.I.) and Glancing Exit (G.E.) scans. Dashes lines represent the desired plane of reflection

For any reflection chosen, symmetric or asymmetric, multiple scans can be performed. Each of these is used to get specific information and depends on the motor controls available.

The first type of scan is an ω:2θ scan (also known as a θ:2θ scan). This is a symmetric scan that is usually performed at the start to verify the materials present and identify the surface orientation. As discussed earlier, ω is at half the value of 2θ. Information from this scan can helps identify if the material or thin-film is single crystal, textured, or polycrystal. The position of the peak (2θ value) can be subsequently used to calculate the lattice parameter from eqns. 3

and 4. For the materials system in study, these scans characterize the (0002) and (0004) peaks for AlN.

The second type of scan is the ω-scan, also known as a rocking curve. In this type of scan, the 2θ motor is kept fixed and only the ω motor is moved about the reflection peak. The sample is tilted around the peak for about 2° on either side. This scan is really important to know how the planes are tilted in the in-plane direction and the mosaic spread of the grains. The more mosaic spread in the material, the greater the FWHM for the curve. The FWHM also depends on the density of dislocations and curvature of the substrate. In general, good-quality films will have a smaller FWHM compared to worse quality thin-films.

The third type of scan that performed is known as a ϕ-scan or an azimuthal scan. For this scan, the detector and sample are fixed at their Bragg angles (ω and 2θ). The sample is then rotated along its surface normal keeping all the other motors fixed. The scan is done from 0° to 360° for a particular reflection. This scan is useful in identifying the multiplicity of a particular plane and whether it is single crystal or not. For example, a (111) oriented cubic thin film if observed under a ϕ-scan for (001) reflection, would only show three peaks separated by 120° instead of 4 peaks separated by 90° each. This is because the film being (111) oriented, there are certain reflection which cannot be accessed. These scans serve as another confirmation on the orientation of a material. ϕ-scans can be used find out how much a thin-film is tilted in-plane (twist) with respect to the substrate by superimposing the two ϕ-scans.

Reciprocal space maps are a convenient way to visualize the crystallographic planes of a material. In reciprocal space, each plane is represented as a point in space, with its distance from the origin inversely proportional to the interplanar spacing. An Ewald sphere indicates all the possible planes that can be observed using a certain wavelength. The constraint comes from Bragg's law itself. Since sin(θ) cannot exceed 1, only planes that have an interplanar spacing of less than or equal to half the wavelength can be observed. Since reciprocal space is in the units of inverse length, the diameter of the Ewald sphere becomes $2/\lambda$. Given below in fig. 9 is the RSM for (0001) AlN when viewed from a $(11\bar{2}0)$ zone axis.

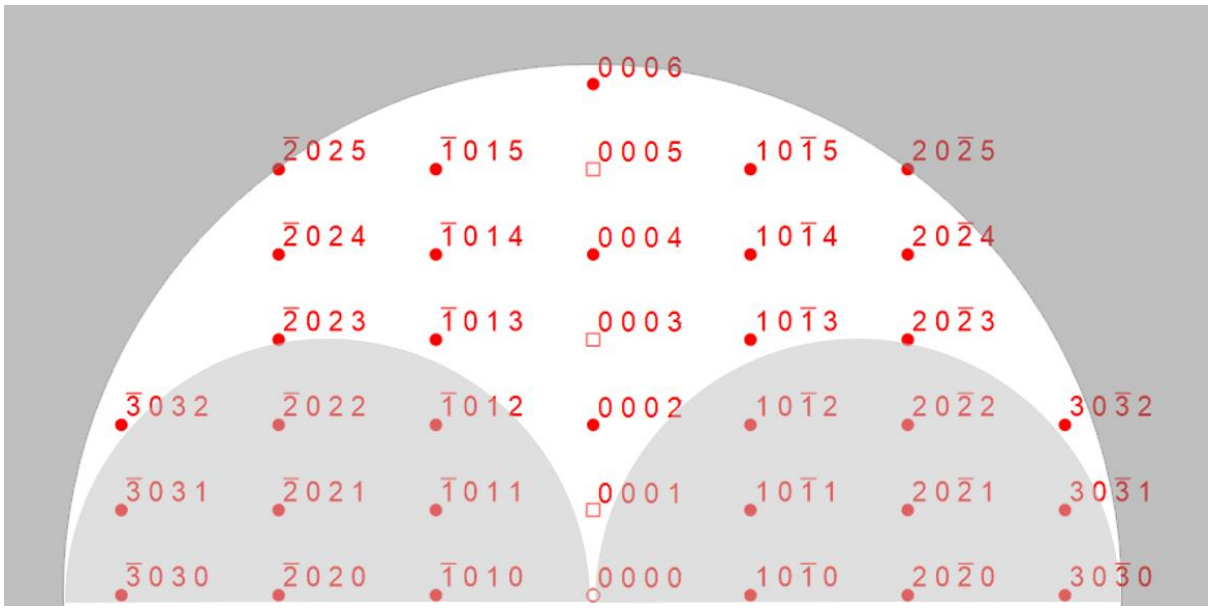

Figure 9: Reciprocal Space Map for (11-20) zone axis (0001) oriented AlN

Fig. 9 shows the points corresponding to crystal planes plotted for a specific zone axis. There are a few things to note about this map. The two semi-circles at the bottom of the RSM cover the region where the planes would be in "transmission." The X-ray beam would have to go through the sample for the peaks there to be observed. Second, some planes have a solid dot while others have an empty square. The empty square represents the planes which have a zero

structure factor (F) and cannot be observed. An optimum reflection plane would not be in the transmission zone and have a high structure factor. For AlN, this corresponds to the (0002) and (0004) peaks for symmetric scans and $(10\bar{1}5)$ for asymmetric scans. In further sections, the substrate and thin-film reciprocal maps have been superimposed to find their relative positions and used to collect the data.

2.3 X-Ray Reflectivity (XRR)

X-Ray Reflectivity is an analysis technique used to characterize the surface of a material. The angle of incidence ranges from about 0° to 4-6° depending on sample complexity. The idea behind this technique is to characterize the surface for its roughness. But since X-rays can have a deep penetration depending on the material, XRR can also be used for finding the roughness at material interfaces, the thickness of thin-films and film density [10].

An important physical characteristic for X-rays is their index of refraction. For X-rays, the index of refraction can be written as given below.

$$n = 1 - \delta - i\beta \tag{5}$$

Where,

n = index of refraction

δ = scattering coefficient

β = absorption coefficient

For most materials, the index of refraction when using x-rays is less than 1. This means that when traveling from air (n = 1) to another material (n < 1), air acts as the denser medium and material acts as the rarer medium. This allows "total external reflection," which is analogous to total internal reflection (TIR) when using visible light [11]. Similar to TIR, the critical angle for total external reflection can also be defined.

$$\cos\theta_c = n = 1 - \delta \tag{6}$$

$$\theta_c^2 = 2\delta \tag{7}$$

Where,

θ_c = Critical angle for total external reflection

Since δ is very small and the critical angle is close to zero, a Taylor expansion can be used to arrive at eqn. 7 using eqn. 6. The term δ is important and relates to the density of the material.

When doing an XRR experiment, it is important to align the sample properly. Since the angle of incidence is very small, the projected length of the incident beam on the sample is very large. The position of the sample within the beam is also important. The beam should hit the surface of the sample and not the side. Keeping the sample flat is also necessary since it will affect the intensity observed and can lead to erroneous conclusions.

Fig. 7 demonstrates simulated XRR data for a 500 nm thick AlN thin film on Si. It compares two cases – smooth AlN thin-film with 0 Å roughness and rough AlN thin-film with 10 Å roughness. The three physical properties of the sample, namely density, roughness and thickness can be calculated using XRR. The simulations have been performed using BEDE Refs software [12].

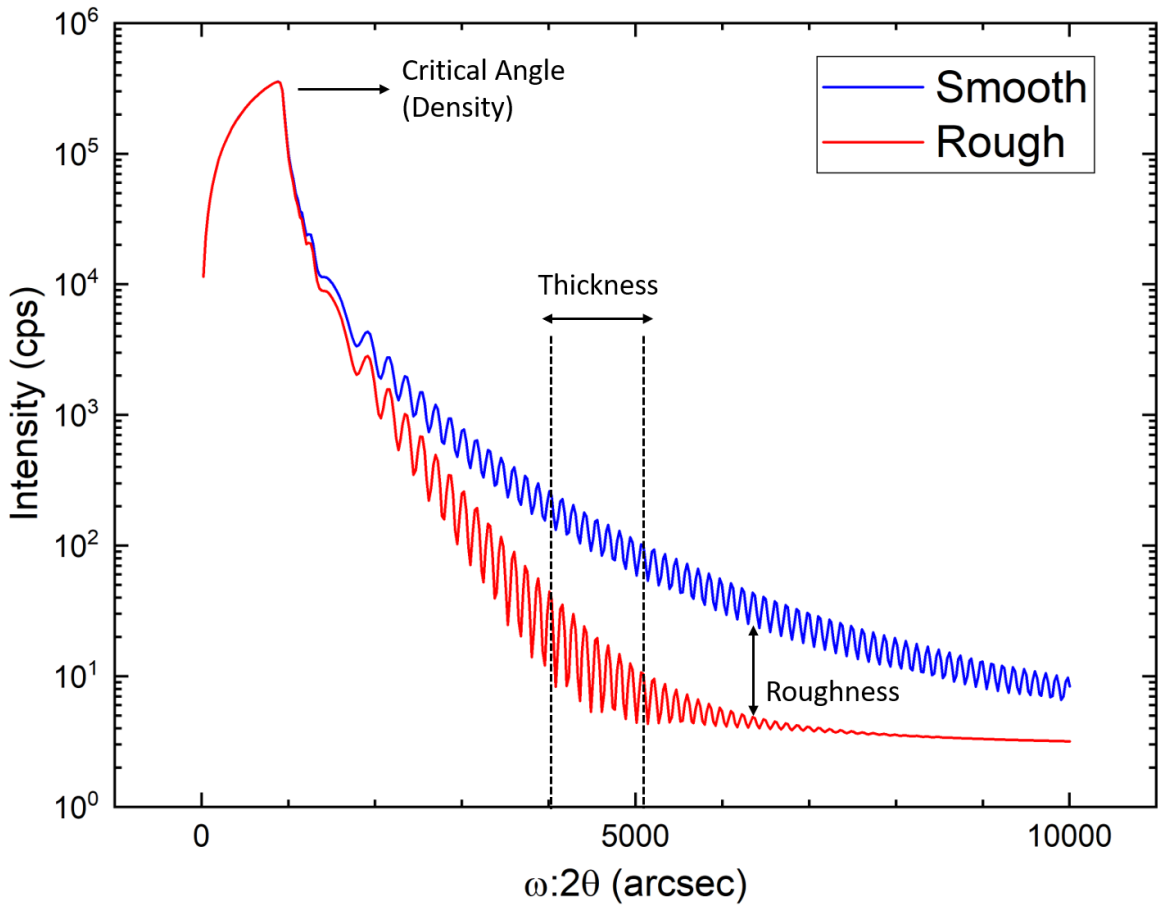

Figure 10: XRR simulation of 500 Å thick AlN thin-film on Si for smooth and rough surfaces

From fig. 7, there are three important features to observe. First is the critical angle peak intensity. Above this angle, total internal reflection is observed. This relates to the scattering coefficient, which, in turn, is related to the density of the material. Second is the drop in intensity for the rough surface. The decrease in intensity is directly proportional to how rough the surface is. For smooth surfaces, the intensity is directly proportional to θ^{-4} [13]. Third are the fringes seen on the tail of the curve. These fringes are related to the thickness of the thin-film. The amplitude of these fringes signifies the difference in densities for the substrate and thin-film. Larger the density difference, larger the fringe amplitude. Eqn. 8 gives the relationship between film thickness and fringe separation.

$$t = \frac{n \,.\, \lambda}{\Delta(2\theta)} \tag{8}$$

$$\theta_m^2 = \theta_c^2 + \left(\frac{\lambda}{2t}\right)^2 m^2 \tag{9}$$

Where,

t = thickness of film

λ = wavelength of x-ray

n = number of fringes

Δ(2θ) = angular separation

m = index of fringe

θ_m = angular position of m^{th} fringe

θ_c = critical angle

Using eqn. 8, and by counting the number of fringes between two points, the thickness can be calculated. Since the fringe spacing might be inconsistent for different points in the actual data, eqn. 9 can also be used to calculate the thickness. By plotting θ_m^2 against m^2, the slope is used to calculate the thickness. All of these calculations can be done computationally by using software like BEDE Refs which models the experimental data and can calculate the density, roughness and thickness for us.

XRR is an excellent technique for characterizing materials for the above properties. Compared to techniques like AFM, which are useful for the characterization of small areas, XRR can be used to characterize bulk surfaces at a go. XRR is also particularly useful for non-destructively characterizing buried interfaces. However, like all techniques, XRR has its

limitations. XRR can only be used for thin-films of thickness up to 300 nm. The resolution for roughness in XRR is about 5 nm. For very high roughness, the intensity has a sharp drop and not enough fringes can be observed. In spite of these limitations, XRR is a powerful technique with no sample preparation required and bulk characteristics measurable. This study uses XRR to analyze AlN thin-films grown on Si.

3 EXPERIMENTAL SETUP

3.1 Sample Information

For this study, two sets of samples have been analyzed. The first set is a collection of four samples with the schematic as shown in fig. 4. The thickness for these samples ranges from 0.3 μm to 1.1 μm. These samples were grown using the MBE technique at various growth temperatures [3]. This approach has been used in recent times to grow GaN directly on Si (111) using nanowire templates [14]. Sample information is listed in table 1.

Sample ID	AlN Thickness (μm)
N550	1.1
N551	0.8
N574	0.8
N635	0.3

Table 1: Sample information for AlN grown on GaN nanowire template

All the above samples were grown on Si (111) with a GaN nanowire on top. The nanowire layer is about a micron thick for all the samples. All the samples are about 1 cm x 1.5 cm in size. The samples are wax mounted on a Si (001) backplate, which is miscut so that it does not interfere with the Si substrate diffraction. The image for sample N635 mounted is shown in fig. 11.

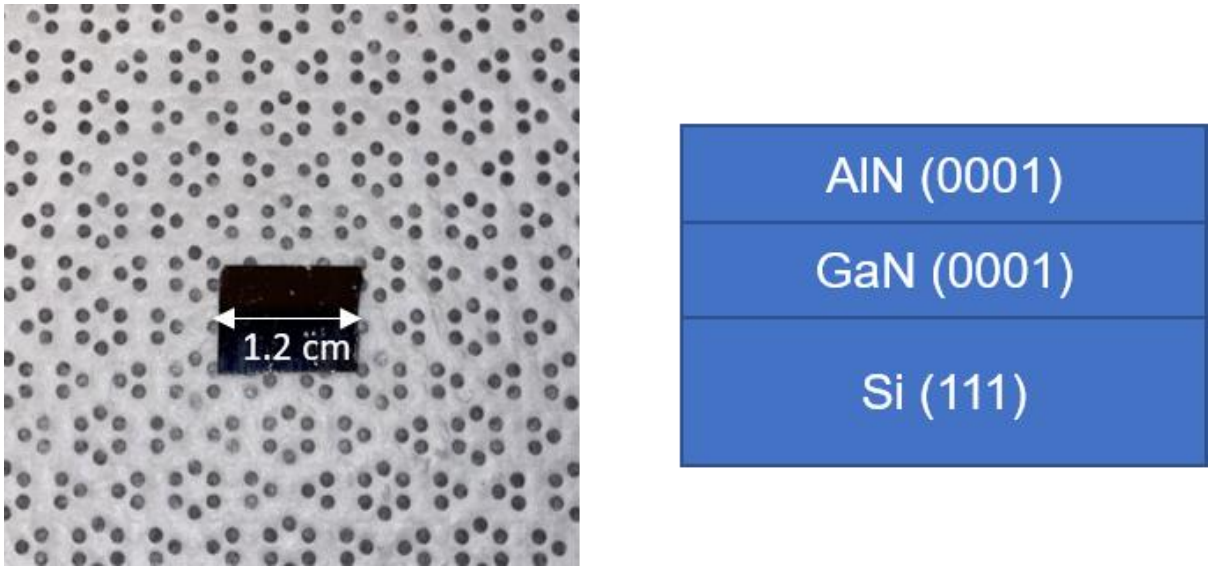

Figure 11: N574 sample mounted on a Si backplate. Dimensions of sample 1cm x 1.2cm

Our second set of samples is AlN thin-film deposited directly on (111) Si. The thickness of the AlN layer is 200 nm. The films have been deposited using Physical Vapor Deposition (PVD) technique. The schematic and image for these samples is given below.

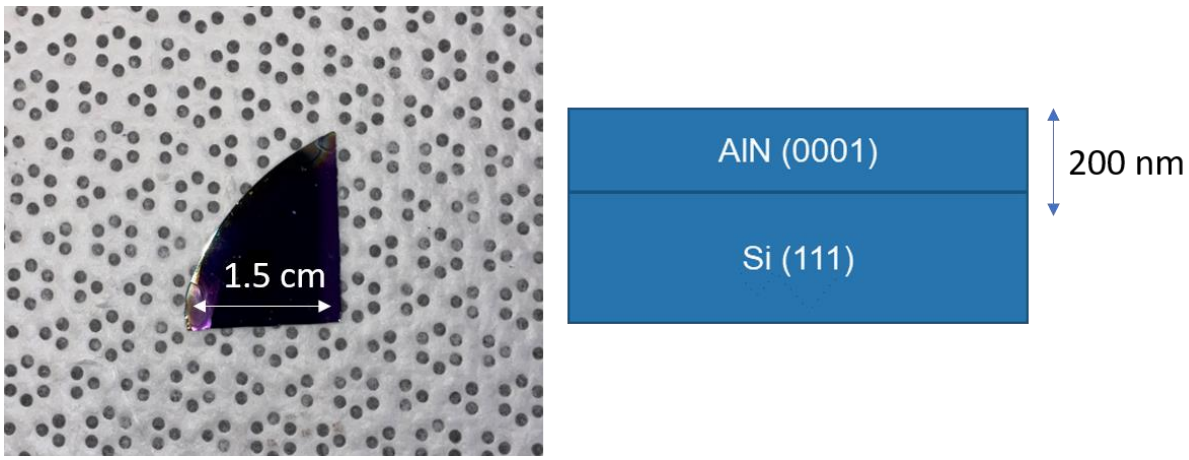

Figure 12: Image and schematic for the second sample, 200nm AlN grown directly on Si

3.2 High-resolution XRD

The equipment used a Bede D1 diffractometer capable of high-resolution triple-axis diffraction (TAD) and double-axis diffraction (DAD). This diffractometer is used to perform strain measurements and map out the reciprocal space for the AlN on Si samples. The schematic for this tool is shown in fig. 13.

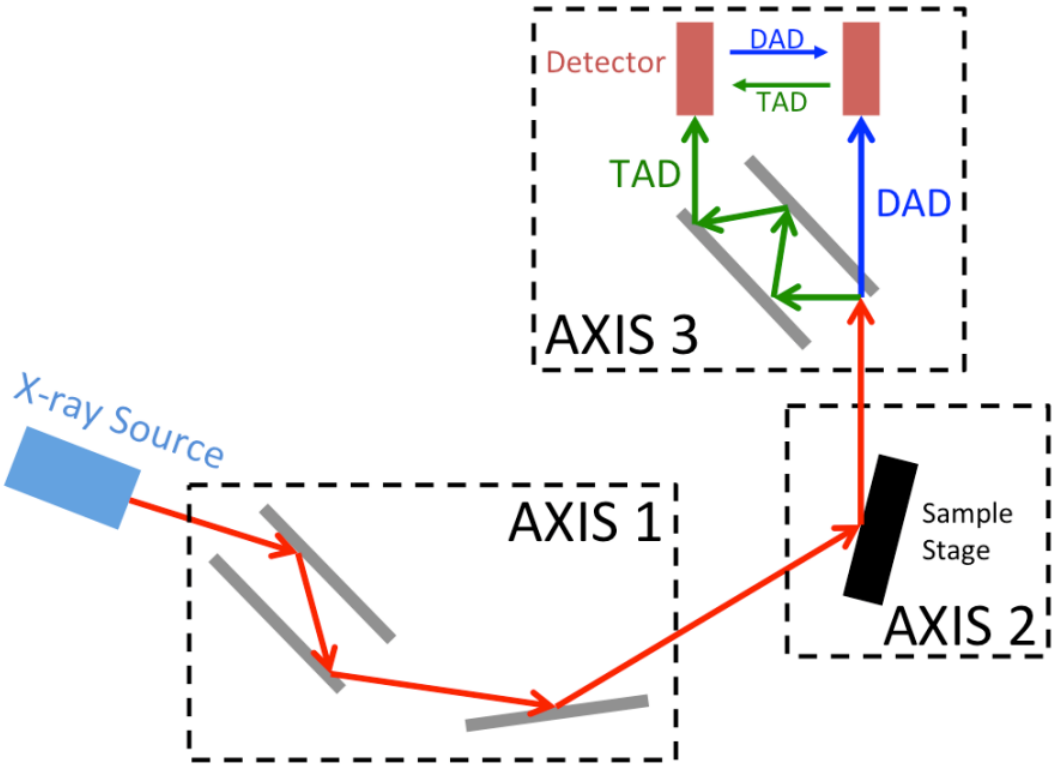

Figure 13: Schematic for high-resolution XRD using BEDE D1 diffractometer [15]

The first axis acts as a monochromator, consisting of a three-bounce channel-cut Si (111) piece. This axis is able to selectively pick out the Cu Kα1 wavelength (λ = 1.54056 Å). The second axis is the sample itself. On the detector side, there are multiple options for analyzer optics. The first is a simple DAD, where the beam passes through a narrow slit and is received on the detector. For TAD, the beam passes through a four-bounce channel cut Si (220). The

resolution of the scan depends on whether TAD or DAD has been used. For DAD, the resolution depends on the slit used. There is another type of detector known as a 1-D detector (Dectris Mythen2 R 1K), which has an array of point detectors spread along a range of 9 degrees in the 2θ direction. This is especially useful for mapping out the reciprocal space since a larger part of the RSM can be captured in a single scan. The resolution for these various techniques is listed in table 2 below.

Slit	Resolution (arcsec)
TAD	10
1-D	32
DAD J1	172
DAD A4	344
DAD A3	688
DAD A2	1375
DAD A1	3438

Table 2: Resolution for the various detector optics available

TAD is used for a long symmetric ω:2θ scan. For finer ω:2θ and ω-rocking curves of individual materials, DAD A4 optics are used. Choosing a higher resolution comes at the cost of the intensity observed. From DAD to TAD, there is a ~1000 times drop in intensity. For measuring RSMs, the 1-D detector is utilized since it can map out the RSMs faster than the point detector and provides good resolution too.

Both symmetric and asymmetric peaks are needed to measure strain in the samples since a hexagonal lattice has two distinct lattice parameters. For AlN, (0002) and (0004) peaks

are observed as the symmetric peaks and $(10\bar{1}5)$ as the asymmetric peak. For both AlN and GaN, the same set of peaks are observed. Figure 14 depicts the RSM for GaN superimposed on AlN. Red dots represent AlN peaks, while black dots represent AlN peaks. Since GaN has a larger lattice parameter than AlN, it appears closer to the origin (lower interplanar distance) than AlN.

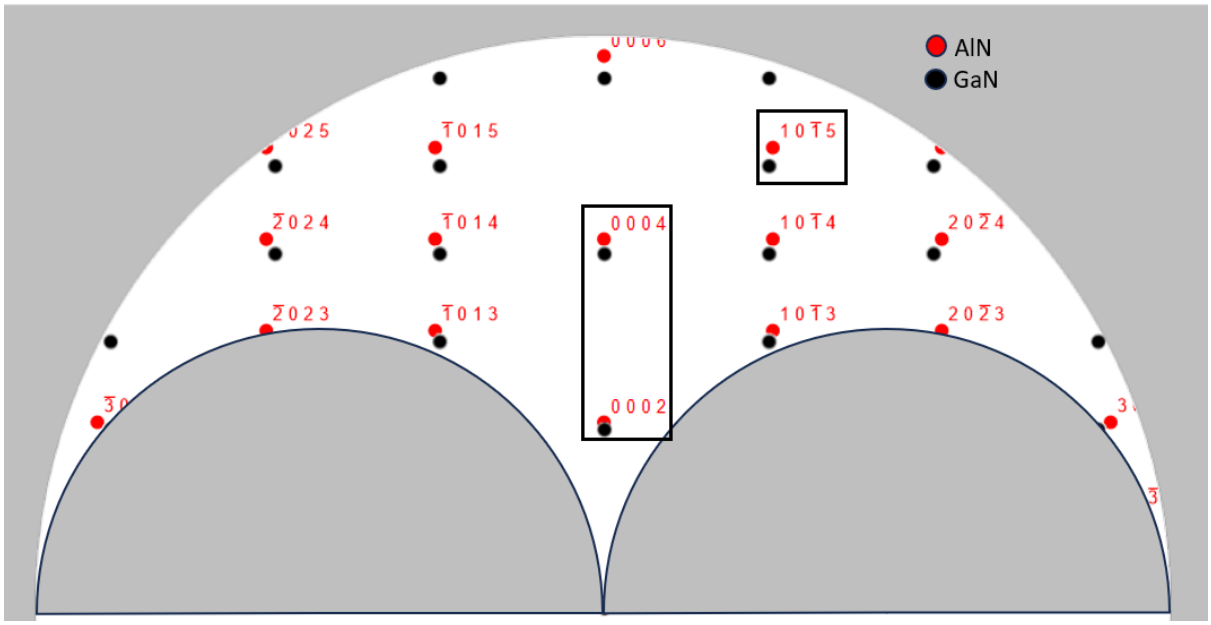

Figure 14: Superimposed RSMs for AlN and GaN with zone axis $(11\bar{2}0)$

4 RESULTS AND ANALYSIS

4.1 Strain Calculations

Calibration of the diffractometer is specifically important for strain measurements where misalignment in any angle can lead to erroneous results. For this reason, Si has emerged as the choice material since high purity single crystal samples are easily available. Silicon powders are also widely used as a calibration material [16]. For all samples, the machine is calibrated using a Si substrate, assuming that the substrate is strain-free and all strains are calculated with respect to the substrate. Samples are also mounted on a miscut and misoriented Si backplate so that the mounting stage does not interfere in the measurements.

The first scan done is a 2θ:ω symmetric scan to verify the materials present in the sample. Figure 15 below depicts a symmetric scan running from 28° to 37°. The Si (111), GaN (0002), and AlN (0002) peaks are present. The scan was performed in triple-axis diffraction mode (TAD) with the analyzer crystal in place. There are a couple of conclusions from this measurement. First, it verifies the materials present in the sample. Second, it confirms the surface orientation of the materials present. The Si is (111) oriented, while the GaN and AlN are (0001) oriented. The materials are also single crystal, as is evident by the lack of asymmetric peaks in the symmetric scan. A textured or polycrystalline sample would have other planes diffracting in a symmetric scan.

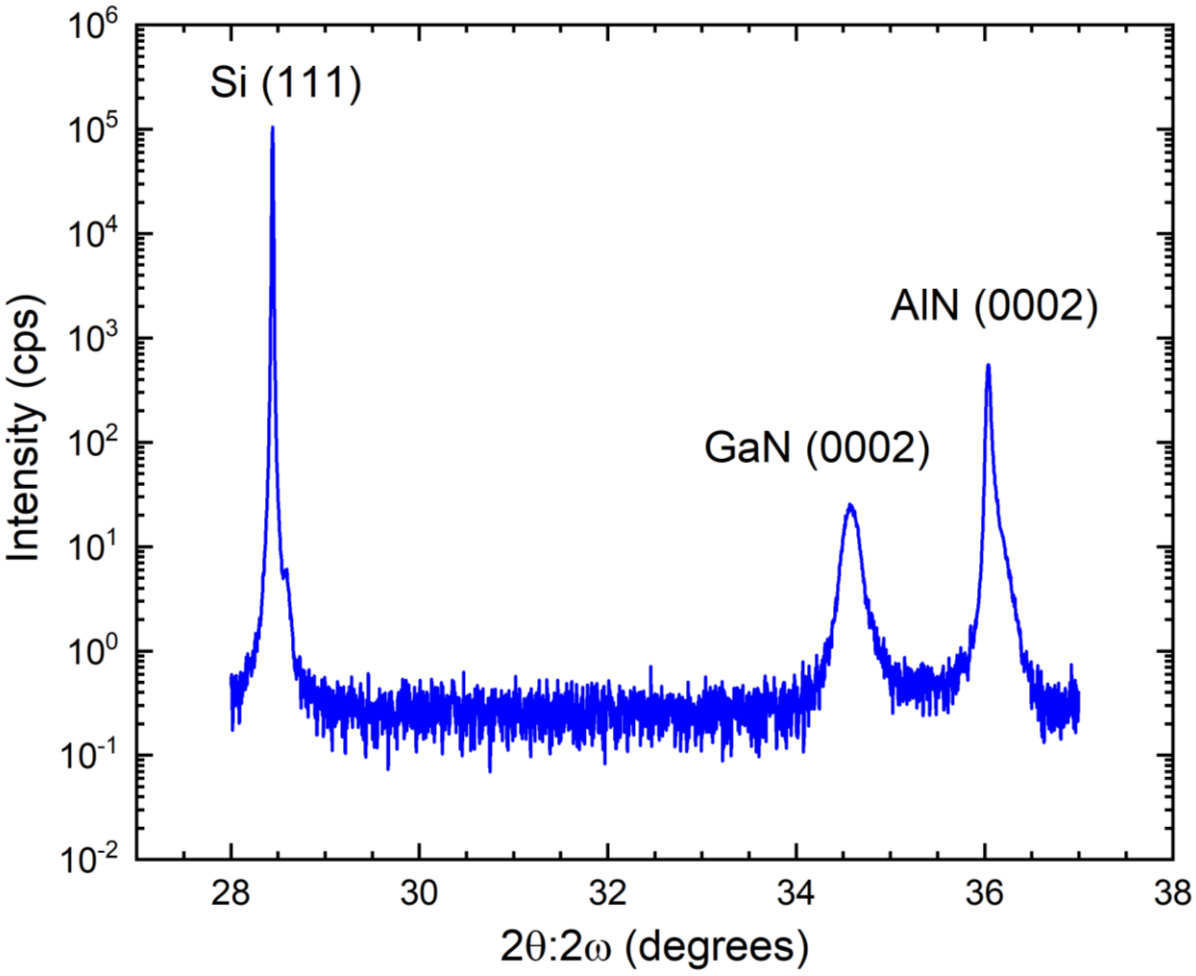

Figure 15: Symmetric 2ϑ:ω scan for sample N574 done in triple-axis diffraction (TAD)

Shorter ranges with smaller step sizes for the individual peaks are performed. These are used to determine the strain in the thin-films.

Figure 16 depicts the ω:2θ scan for the Si (111) peak for the N574 sample performed in DAD using the A4 slit. Sample N574 is used as an example of how the strain values were calculated. As a rule of thumb, the step size is chosen to be less than or equal to $1/7^{th}$ of the FWHM. The ω and 2θ on the machine are set to the Si peak for calibration. Apart from these, the χ motor is also adjusted to get maximum peak intensity.

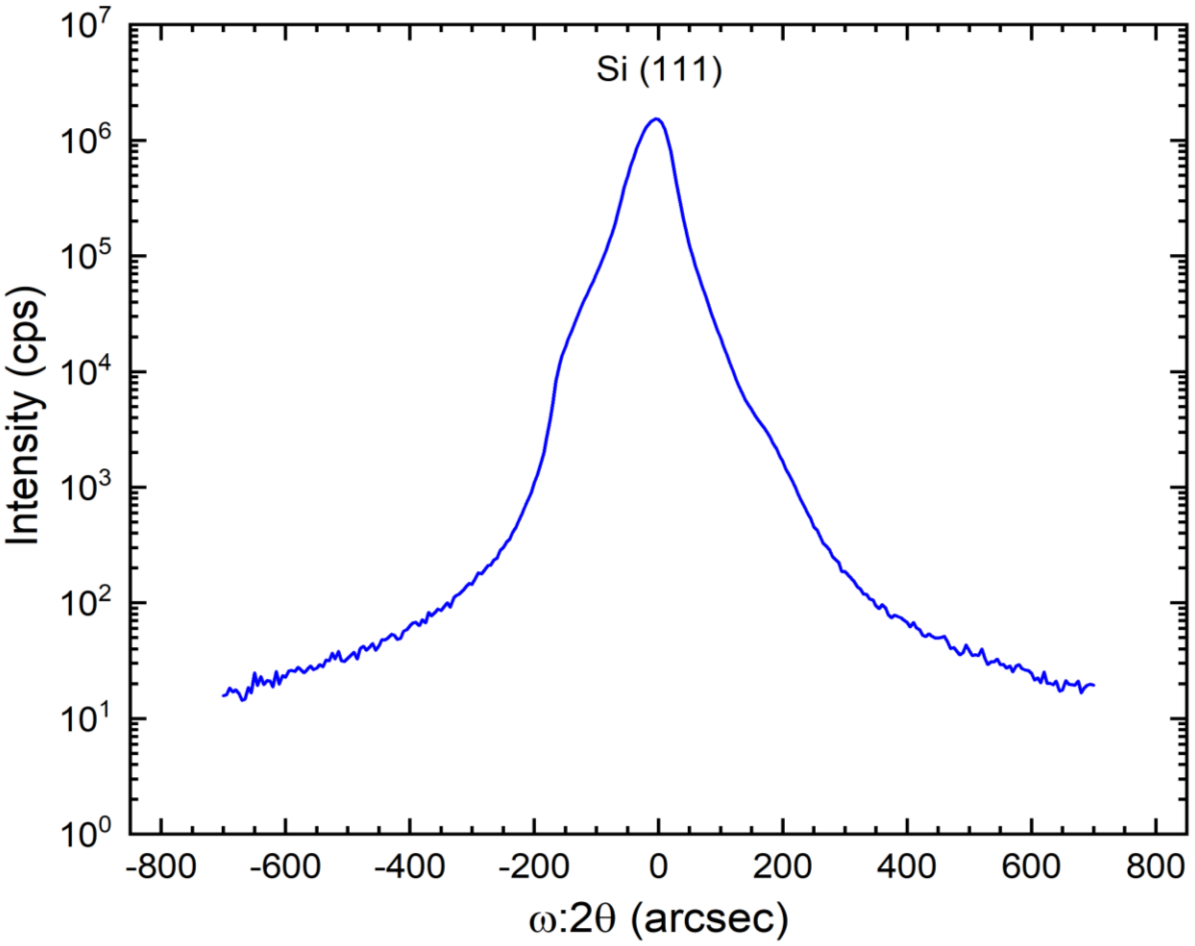

Figure 16: ω:2ϑ scan for Si (111) peak for N574 sample done in DAD

Once the equipment is calibrated, the AlN (0002) peaks are analyzed with the ω:2θ and ω-rocking curve measurements. The Bragg angle for the AlN (0002) peak is 2θ = 36.0401°. Since AlN might be strained and not perfectly crystalline (presence of defects), the peak may not be at the exact angle. A long ω:2θ scan captures all the peaks present. Figure 17 shows the ω:2θ for the AlN (0002) peak.

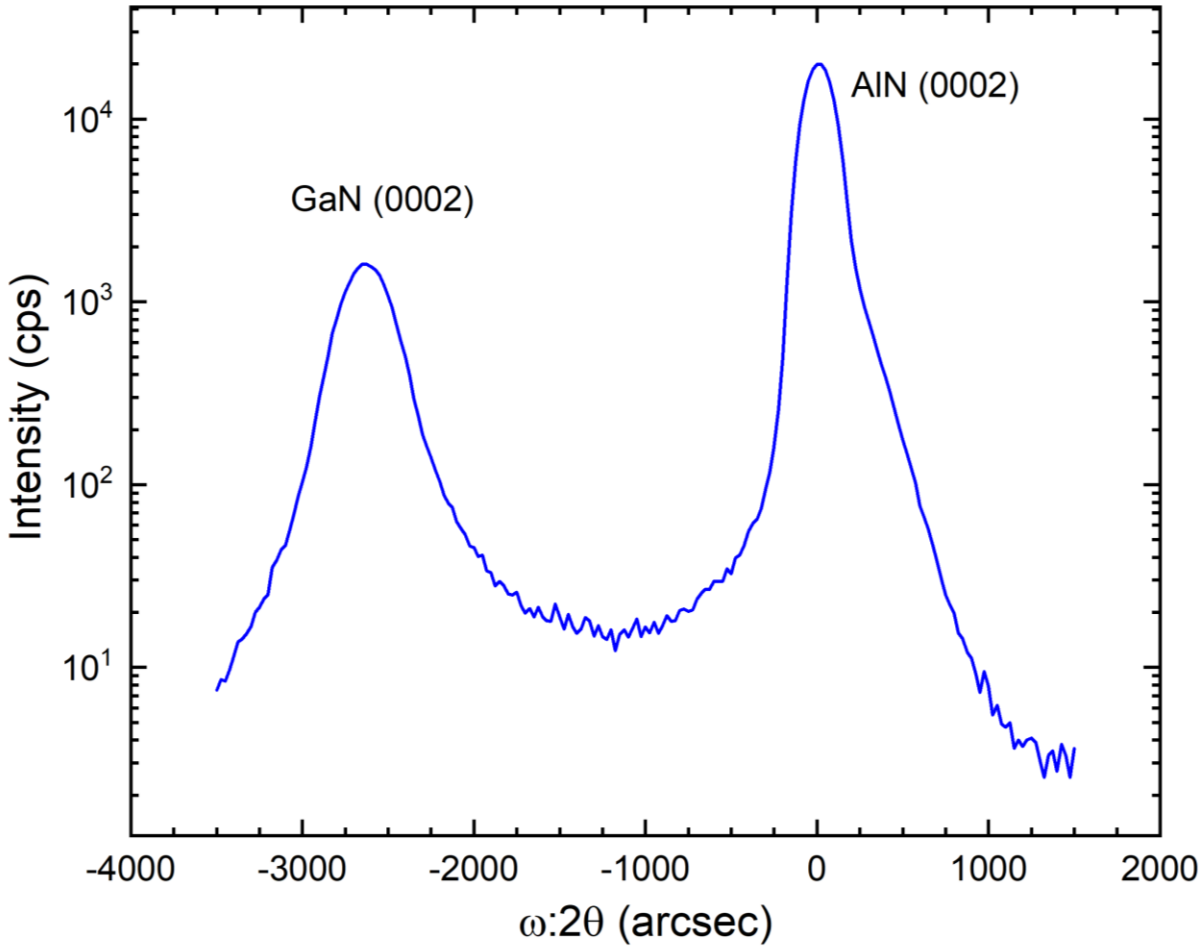

Figure 17: ω:2ϑ scan for AlN (0002) and GaN (0002) peaks for sample N574

The GaN (0002) peak is observed at a lower Bragg angle than AlN. The ideal Bragg angle for GaN (0002) is 2θ = 34.5418°. Since GaN has a bigger lattice parameter than AlN, in reciprocal space, the interplanar distance becomes smaller (eqn. 3), resulting in a lower Bragg angle. These symmetric scans are used to calculate the out-of-plane lattice parameter (c) and the out-of-plane strain.

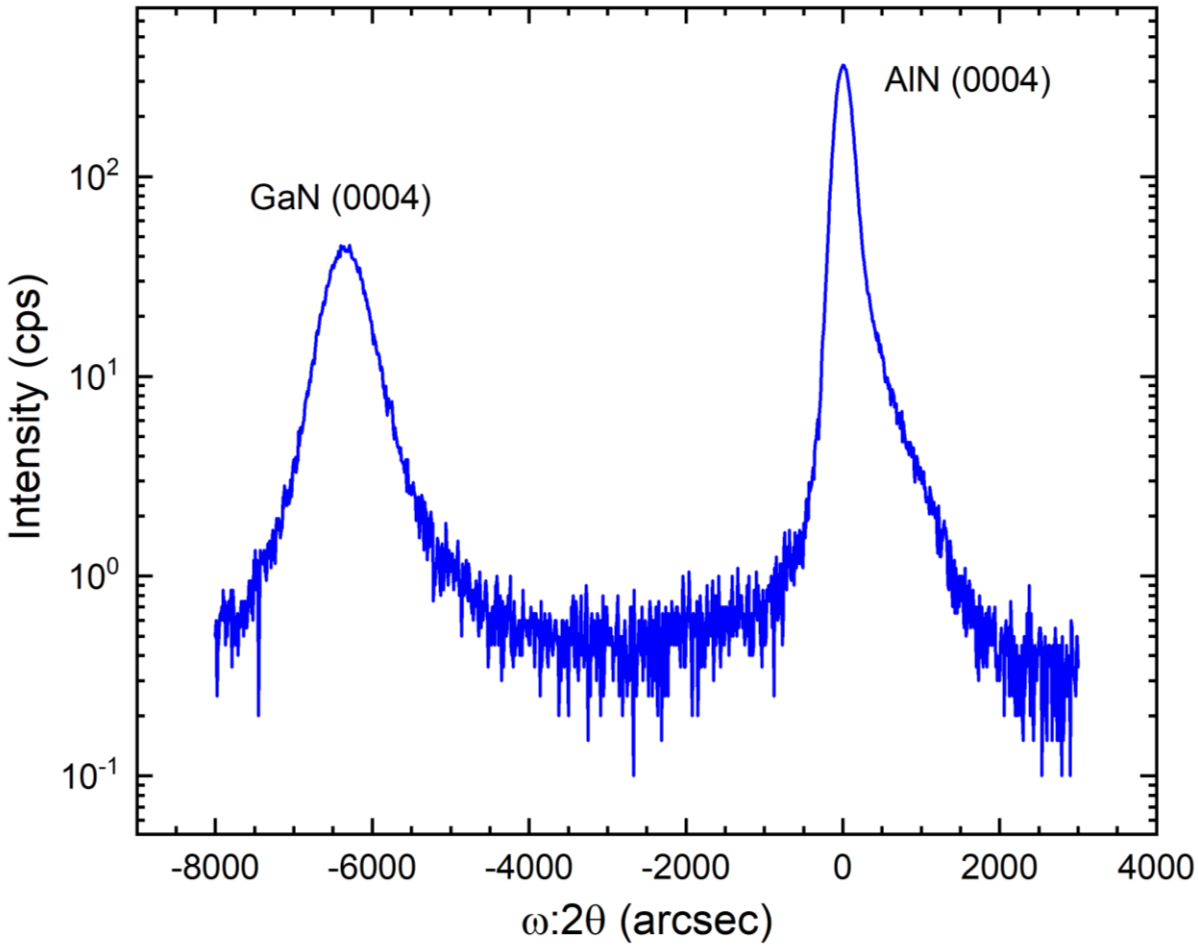

Figure 18: ω:2θ scan for AlN (0004) and GaN (0004) peaks for sample N574

Figure 18 depicts the AlN (0004) and GaN (0004) scan. Compared to the (0002) peaks, these have a lower intensity. This is due to a lower scattering factor at higher angles.

Strain is determined using the following formula:

$$Strain\ (\%) = \frac{Ideal\ lattice\ parameter - Measured\ lattice\ parameter}{Ideal\ lattice\ parameter} * 100 \quad (10)$$

Calculation of out-of-plane strain:

For AlN (0002),

Peak 2θ value (from fig. 17) = 36.0246°

Using eqn. 1 (Bragg's Law), inter-planar spacing (d) = 2.491 Å

Using eqn. 3, out-of-plane lattice parameter (c) = 4.982 Å

For AlN (0004),

Peak 2θ value = 76.4326°

Inter-planar spacing (d) = 1.245 Å

Out-of-plane lattice parameter (c) = 4.980 Å

Average out-of-plane lattice parameter (c) = 4.981 Å

Ideal out-of-plane lattice parameter [2] = 4.981 Å

Strain = 0%

Calculation of out-of-plane strain:

For GaN (0002),

Peak 2θ value = 34.5663°

Inter-planar spacing (d) = 2.593 Å

Out-of-plane lattice parameter (c) = 5.185 Å

For GaN (0004),

Peak 2θ value = 72.9104°

Inter-planar spacing (d) = 1.296 Å

Out-of-plane lattice parameter (c) = 5.185 Å

Average out-of-plane lattice parameter = 5.185 Å

Ideal out-of-plane lattice parameter = 5.189 Å

Strain = 0.08%

Similar calculations for all the other samples are performed and out-of-plane lattice parameters and strains are calculated. To calculate the in-plane strain, the asymmetric peaks are measured. For both AlN and GaN, the $(10\bar{1}5)$ peaks are observed. The scans are performed using the 1-D detector, and RSMs for all samples have been generated. For N574, the RSM for $(10\bar{1}5)$ peak has been shown below.

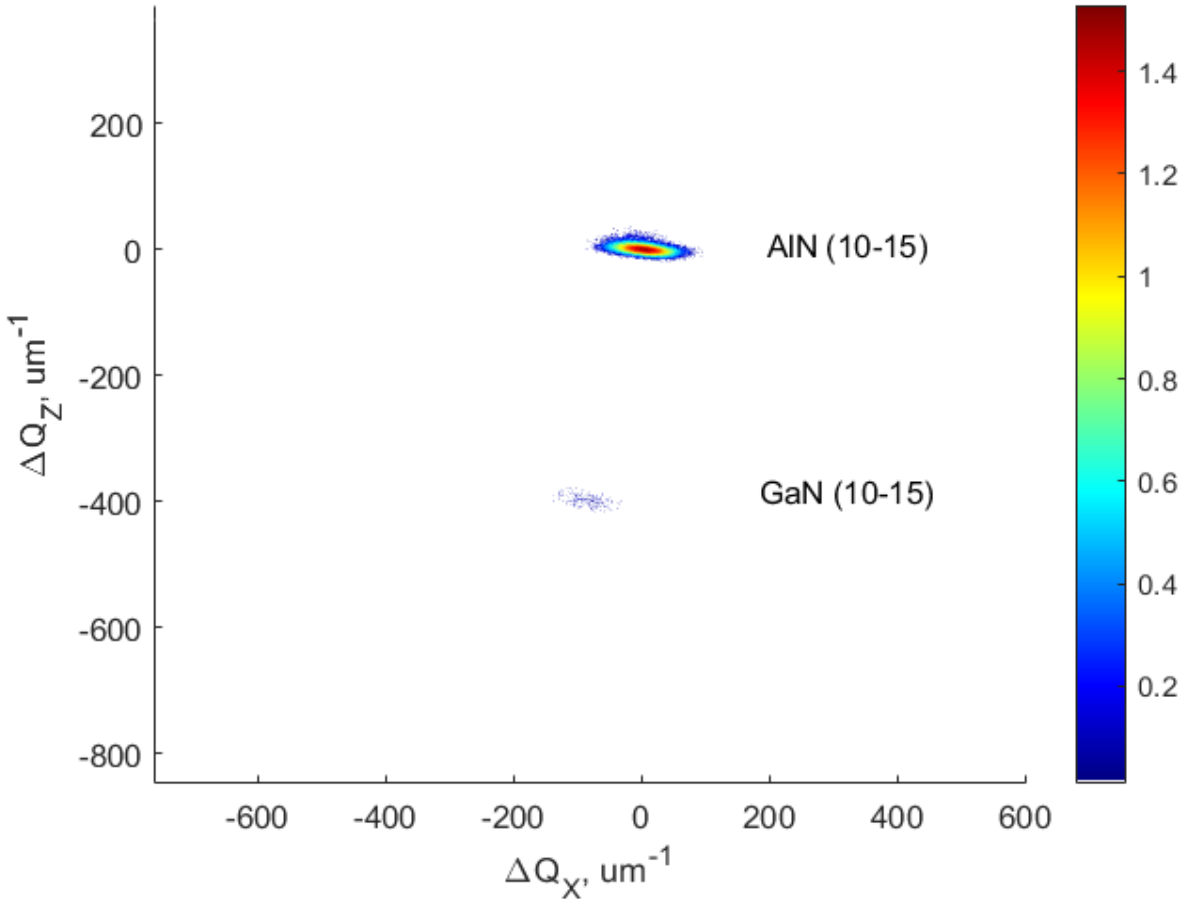

Figure 19: Reciprocal space map for AlN and GaN (10-15) peak for N574 sample

Figure 19 depicts the reciprocal space map in relative units with the origin fixed at AlN peak intensity. AlN has a higher intensity than GaN, and is stretched out in the horizontal (Qx) direction. Following a process similar to the out-of-plane calculations, the in-plane strain for

both these materials are calculated. Using Bragg's law and eqn. 3, the strain for AlN and GaN is 0% and -0.31%, respectively. A positive strain indicates that the unit cell is being compressed with respect to the ideal cell, while a negative strain indicates the opposite. Figure 20 and 21 below depict in-plane and out-of-plane strain respectively.

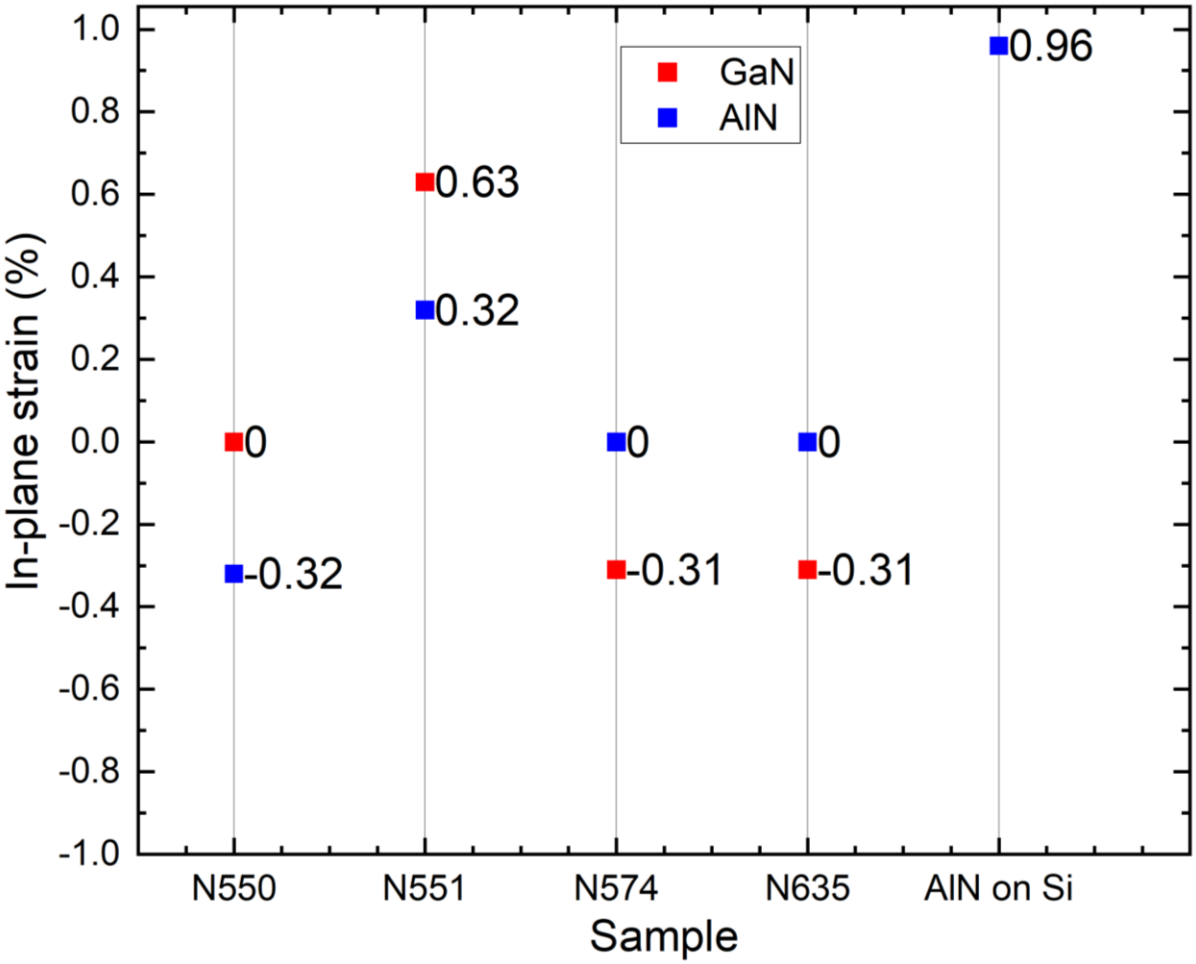

Figure 20: Calculated in-plane strain for AlN and GaN

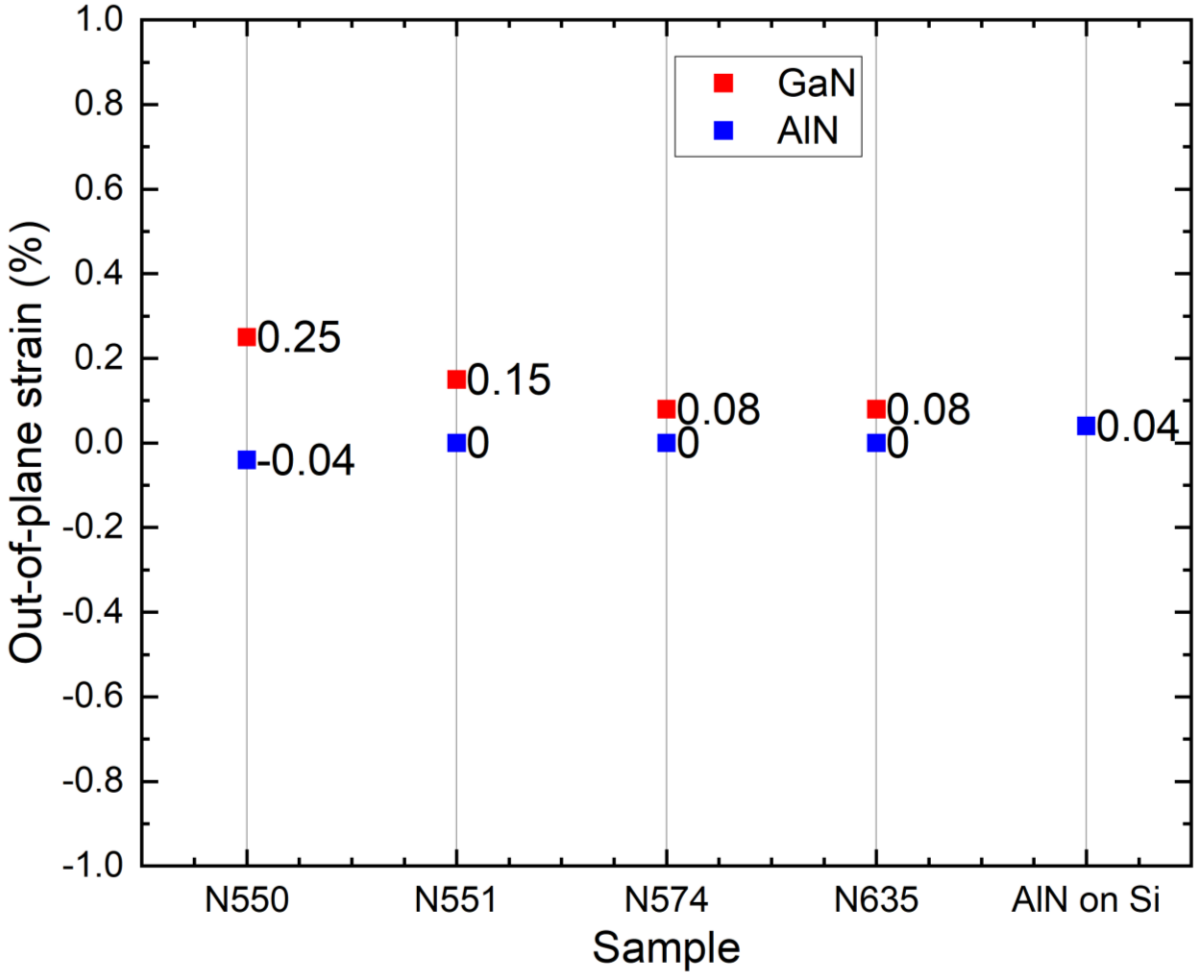

Figure 21: Calculated out-of-plane strain for AlN and GaN

A couple of observations can be made from the strain measurements. First, the AlN layer is virtually strain-free. This is important since electronic applications require high-quality, strain-free thin films [17]. Second, the sample without the GaN nanowire layer has a higher strain for both in-plane and out-of-plane lattice parameters. This shows that the GaN nanowire layer helps reduce strain by creating a layer closer to AlN in lattice parameter than Si. The thicker sample (N550) has a higher strain. As mentioned in the next section, the same sample also has a higher FWHM in the rocking curve, indicating lower film quality possibly due to defects.

The RSMs for AlN and GaN (0002) and (0004) peaks are given below for reference. These can also be used to generate the same ω:2θ and ω-rocking curves seen earlier. Looking at the shape of the RSM, the broadening direction of the peak can be figured out, mosaicity or sub-grains of coherence length in the sample.

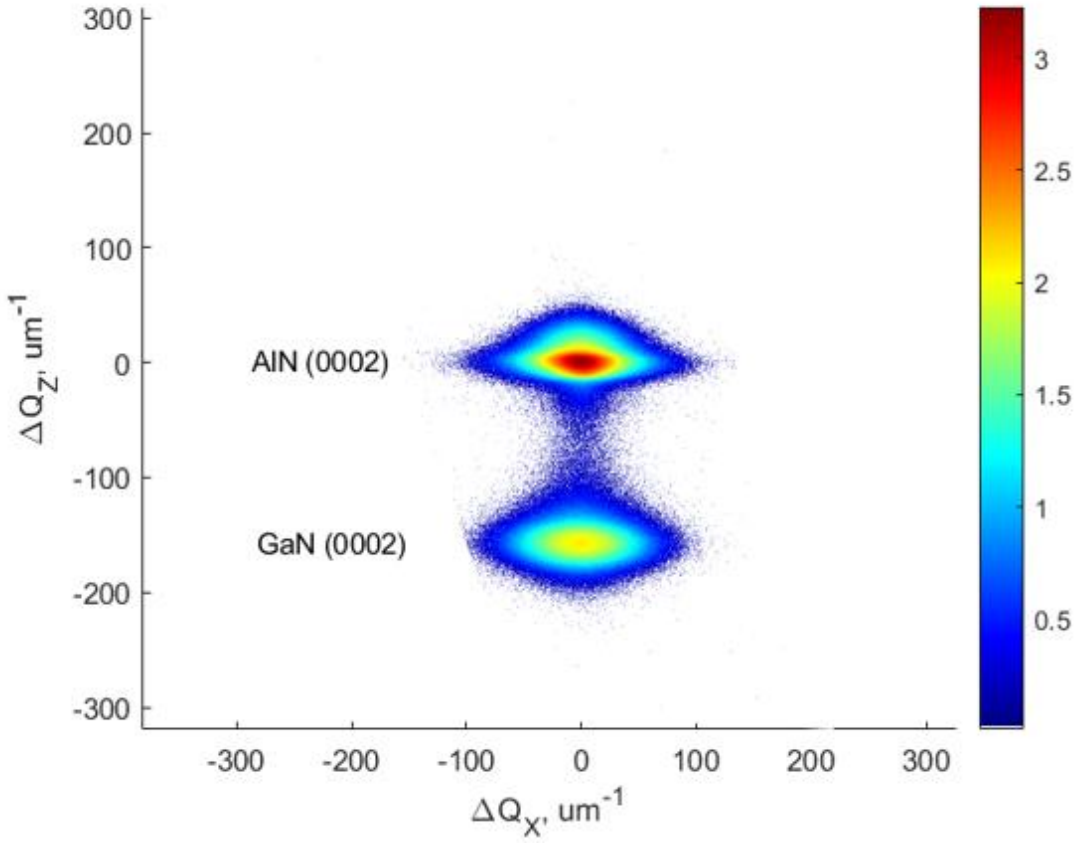

Figure 22: Reciprocal space map for AlN and GaN (0002) peaks taken on a 1-D detector

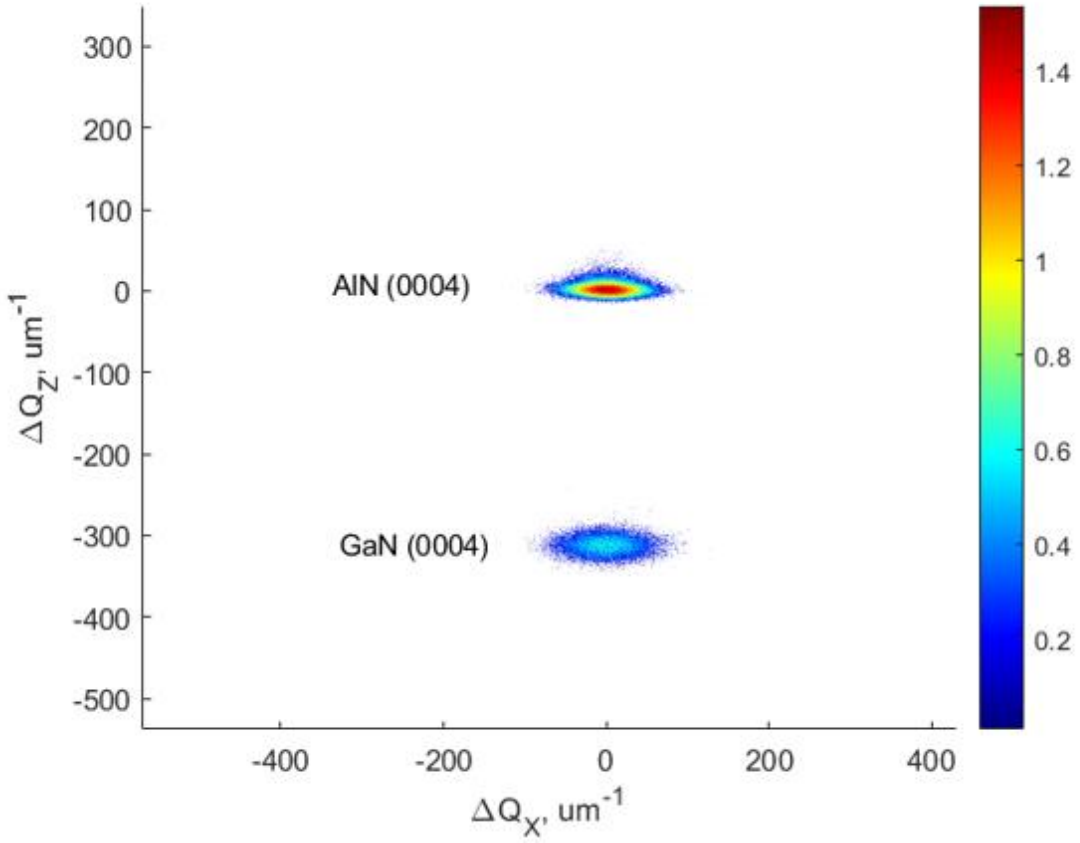

Figure 23: Reciprocal space map for AlN and GaN (0004) peaks taken on a 1-D detector

Both the RSMs show a clear broadening in the horizontal direction. For symmetric scans, this direction can be Qx or ω direction. The asymmetric RSM shows that the peak is tilted in the ω direction. The implications of this have been explained in the next section. Also, the presence of streaks in the (0002) RSM is an artifact of the finite angular resolution of the detector [18].

4.2 Rocking Curve Analysis

Figure 22 below shows the ω-rocking curve for AlN (0002) and AlN (0004) for the N574 sample. The peaks are intensity-matched and plotted in the relative units (arcsec). The FWHM for both peaks is 1235 arcsecs.

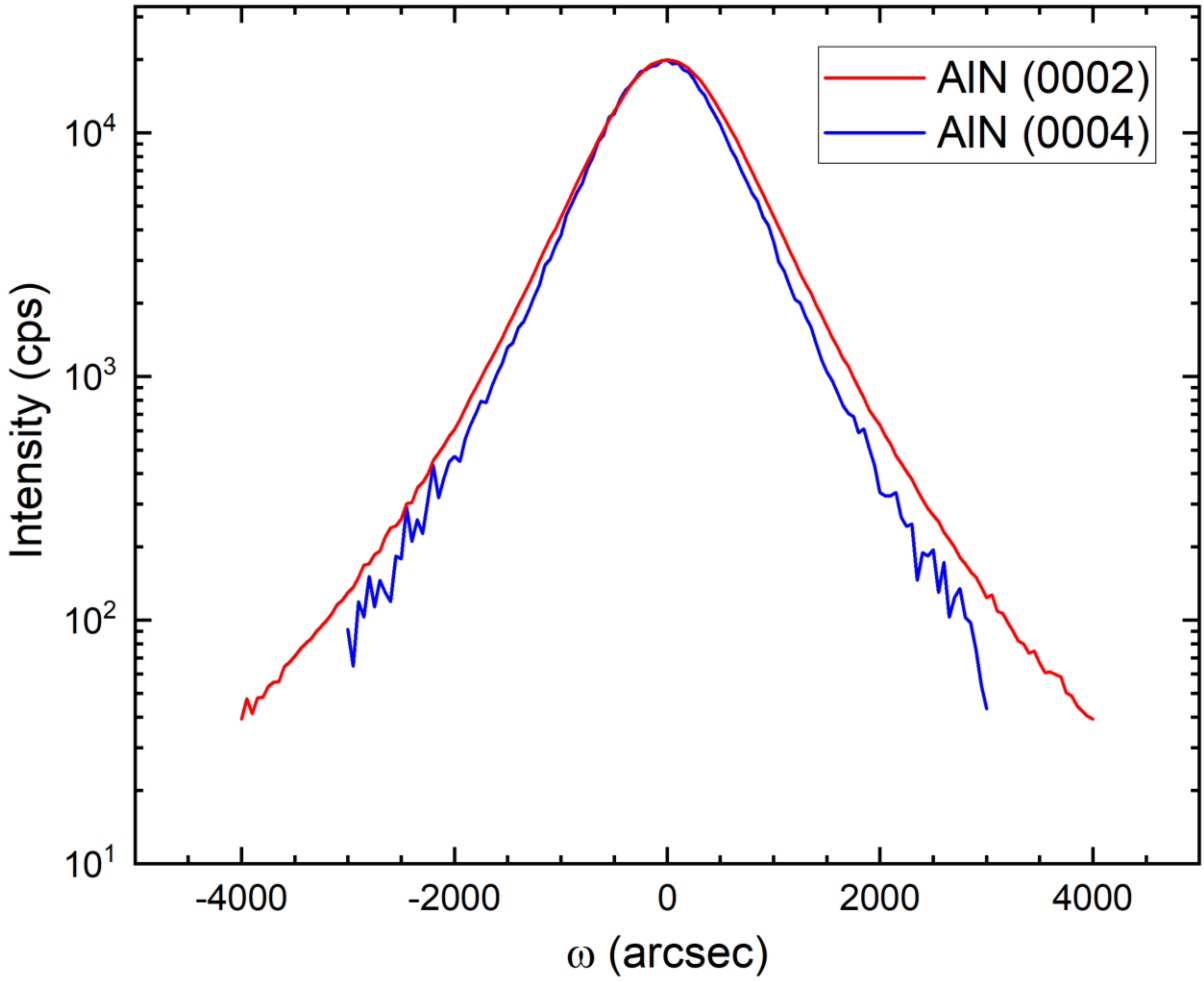

Figure 24: w-rocking curves for AlN (0002) and (0004) curves for the N574 sample

Both the peaks have the same FWHM in angular units. This indicates the presence of mosaicity in the sample, specifically, out of plane tilt. This may be due to the presence of defects or growth conditions for the thin-film.

Figure 23 plots the FWHM for all the samples for both (0002) and (0004) peaks. A clear trend where both the peaks have a similar FWHM (in angular units) is observed. For all the samples, the broadening in the ω-curve can be attributed to mosaicity, specifically out of plane tilt.

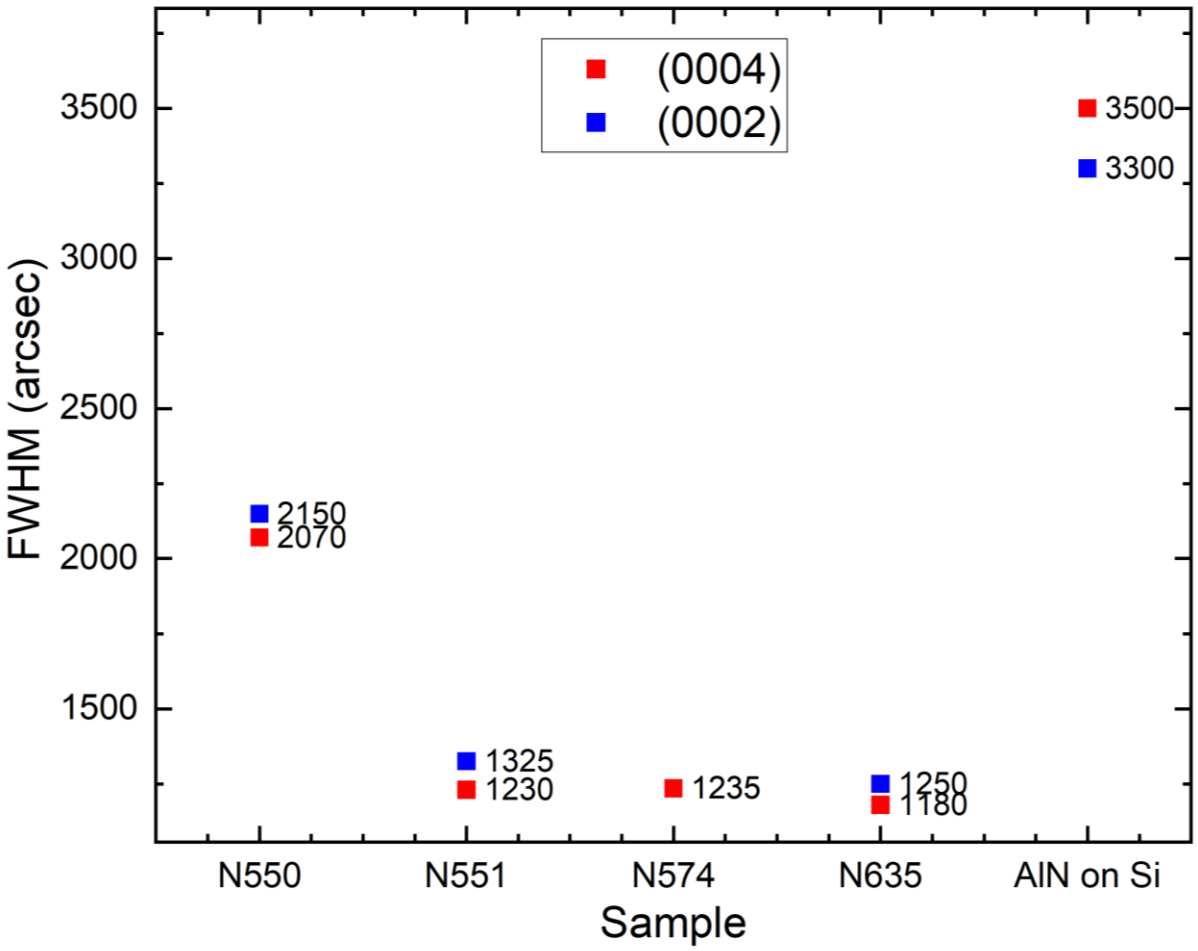

Figure 25: Rocking curve FWHM summarized for all samples

Another important observation is that samples with lower strain values (N551, N574, and N635) have lower FWHM, indicating better film quality. These films are also thinner than N550, which has higher strain and higher FWHM. The sample without the GaN nanowire interlayer has a very high FWHM. This shows that the GaN nanowire layer is important for

reducing the strain and preserving the film quality. For samples with just AlN on Si, surface characteristics also become important.

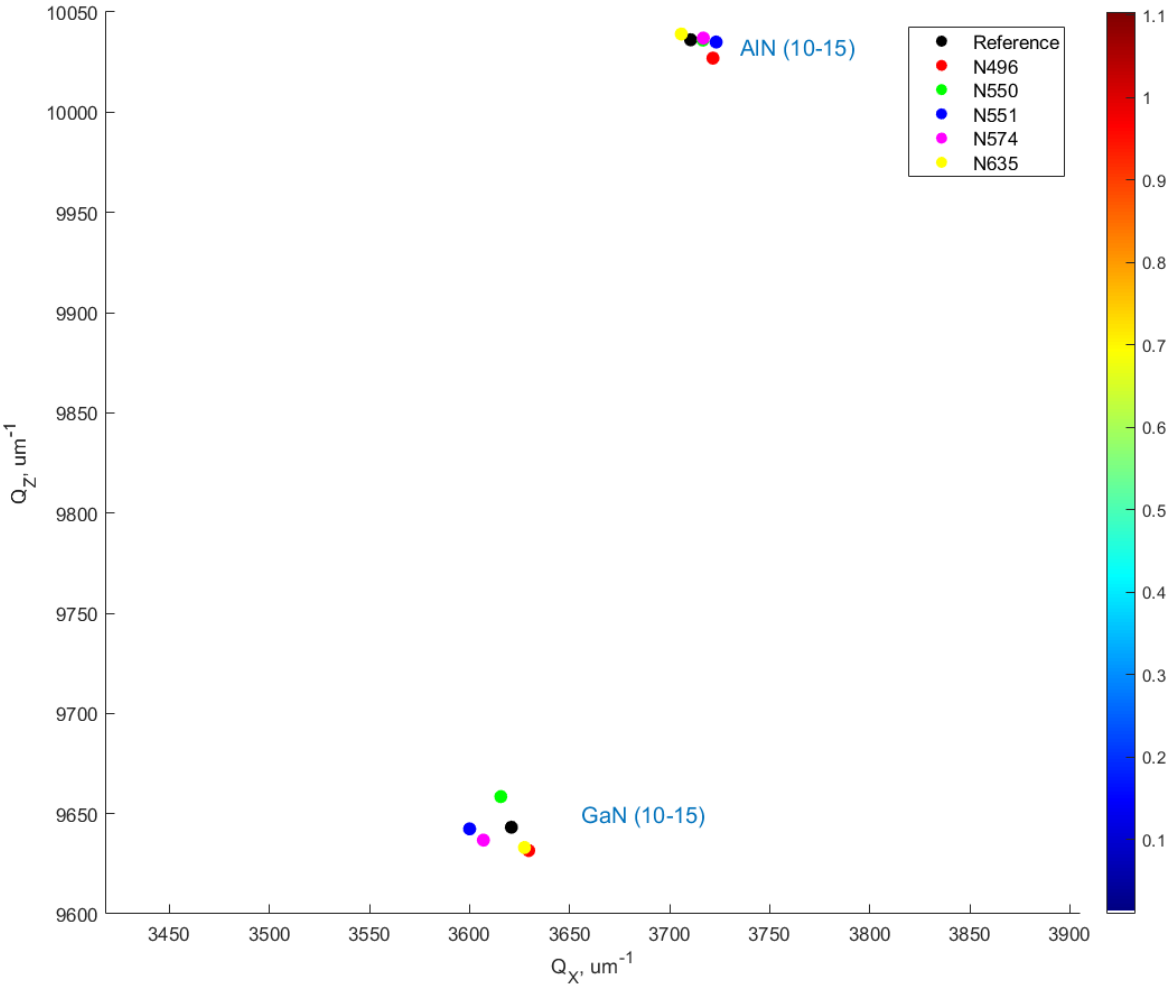

Figure 26: AlN and GaN (10-15) peaks plotted on the RSM along with the reference peak

Figure 26 depicts AlN and GaN (105) peaks plotted with the reference peak. This serves to visualize the strain values. The further away peaks are from the reference, higher the strain. GaN peaks have a higher strain than AlN, also seen in figures 20 and 21. The surface roughness, film thickness, and density of the thin-film have been measured. Results have been presented in the next section.

4.3 XRR and zone axis measurements

Figure 24 depicts the XRR for the AlN on Si sample performed in TAD using the point detector. Sample alignment is crucial for XRR scans since the fringe spacing and intensities are sensitive to the sample position. If incorrectly aligned, the data may show erroneous results. Data from the scan was then fitted into BEDE REFS software. Both the data and model curves are shown in fig. 24.

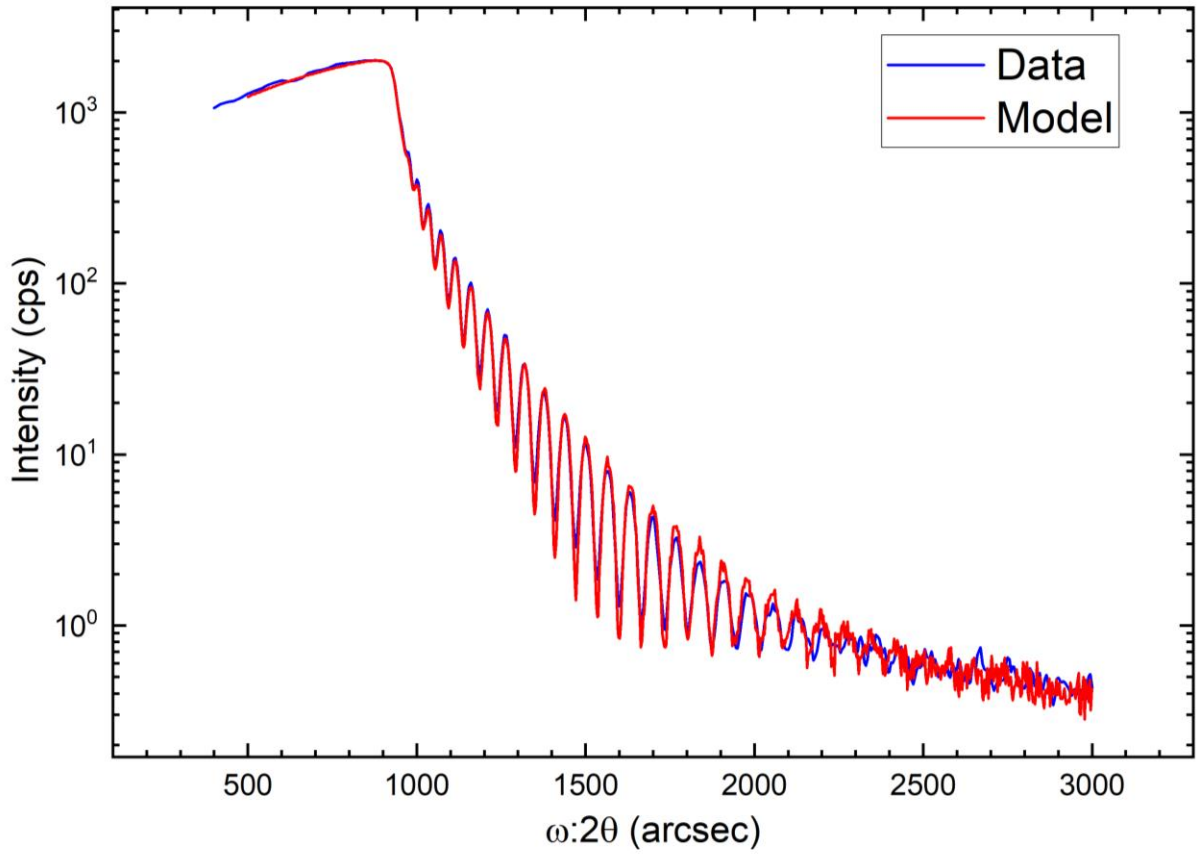

Figure 27: XRR scan for AlN on Si sample along with model data from BEDE REFS

Results from the model fit are as follows. The thickness for AlN is 196 nm, compared to the expected 200 nm from deposition. The surface roughness is 3.2 nm. This is the average roughness of the entire surface compared to the spot roughness measured in AFM. The

calculated density for AlN is 3.26 g/cm^3, or 99% of the ideal density. XRR also allows the study of buried interface of Si. From the model calculations, the roughness of the Si interface comes out to 0 nm (negligible roughness). The density for Si is 2.328 g/cm^3, or 97% of the ideal density. XRR data confirms that the film is about 200 nm thick and gives the roughness of the top surface.

The next figure shows the φ-scans (azimuthal scans) for AlN ($10\bar{1}3$) and Si (220). Both are asymmetric peaks for the materials. These scans confirm the single crystal nature of the materials and find out if any texturing is present. Six distinct peaks for AlN ($10\bar{1}3$) are observed, indicating a single crystal sample. The six peaks are characteristic of a hexagonal lattice. For Si, three distinct peaks for the three-fold (111) symmetry of the substrate are seen.

To perform Transmission Electron Microscopy (TEM) measurements, the orientation of the samples, in and out-of-plane must be known. The surface orientations for both are known. Si (111) is parallel to the AlN (0001) plane. For in-plane directions, the [$10\bar{1}0$] direction in AlN is parallel to the [$11\bar{2}$] Si direction. Literature has reported similar orientation growths for AlN thin films sputtered on (111) oriented Si substrates [19].

Figure 26 shows the long 2θ:ω scan for the AlN on Si sample, confirming the single crystal nature of both materials. An interesting feature of this scan is the presence of Si (222) peak, which is forbidden by structure factor. The peak shows up because multiple reflections are added up from different allowed vectors, resulting in the (222) diffraction vector [20]. This is very sensitive to the azimuthal angle (φ) and can be detected for only very specific values.

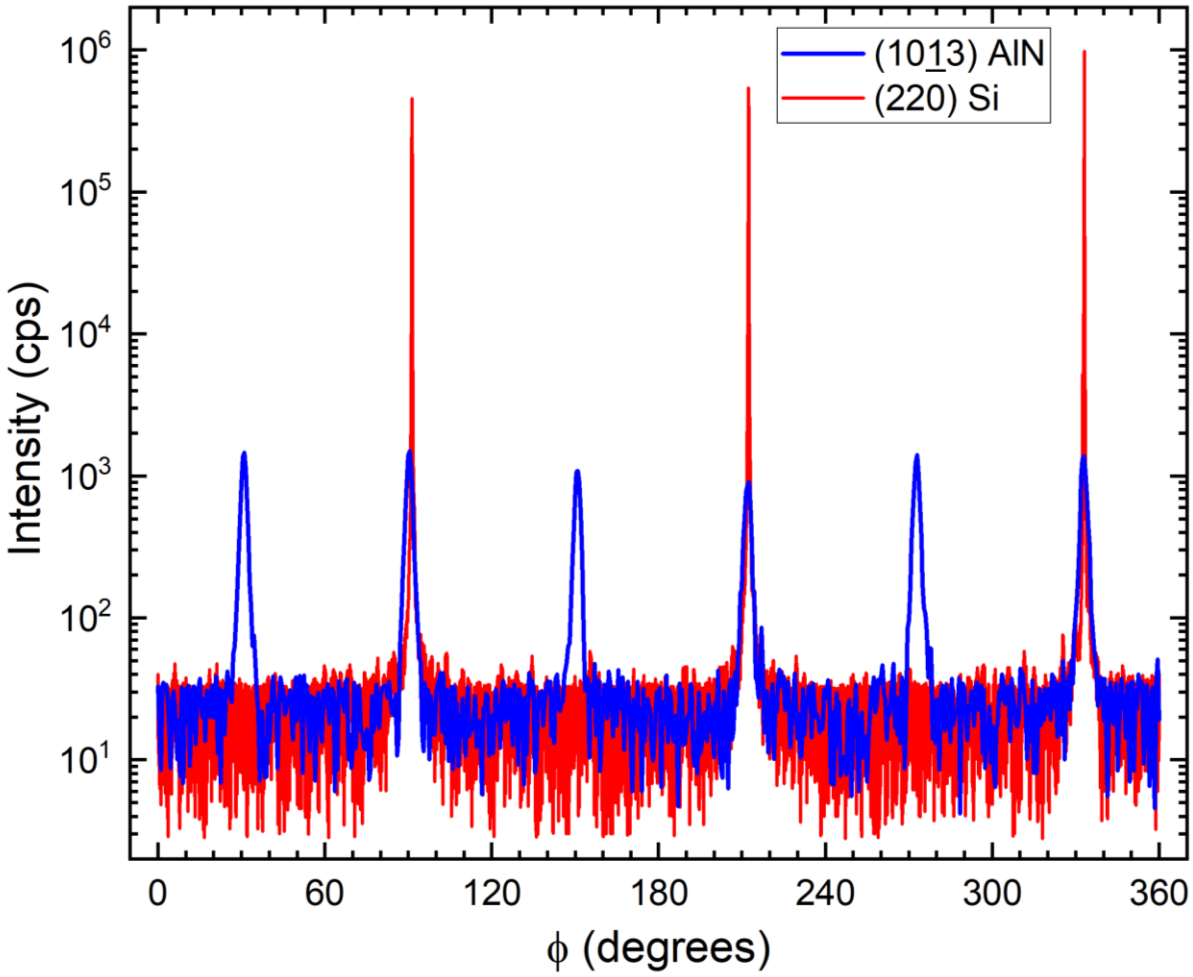

Figure 28: Phi scans for AlN (10-13) and Si (220) for AlN on Si sample

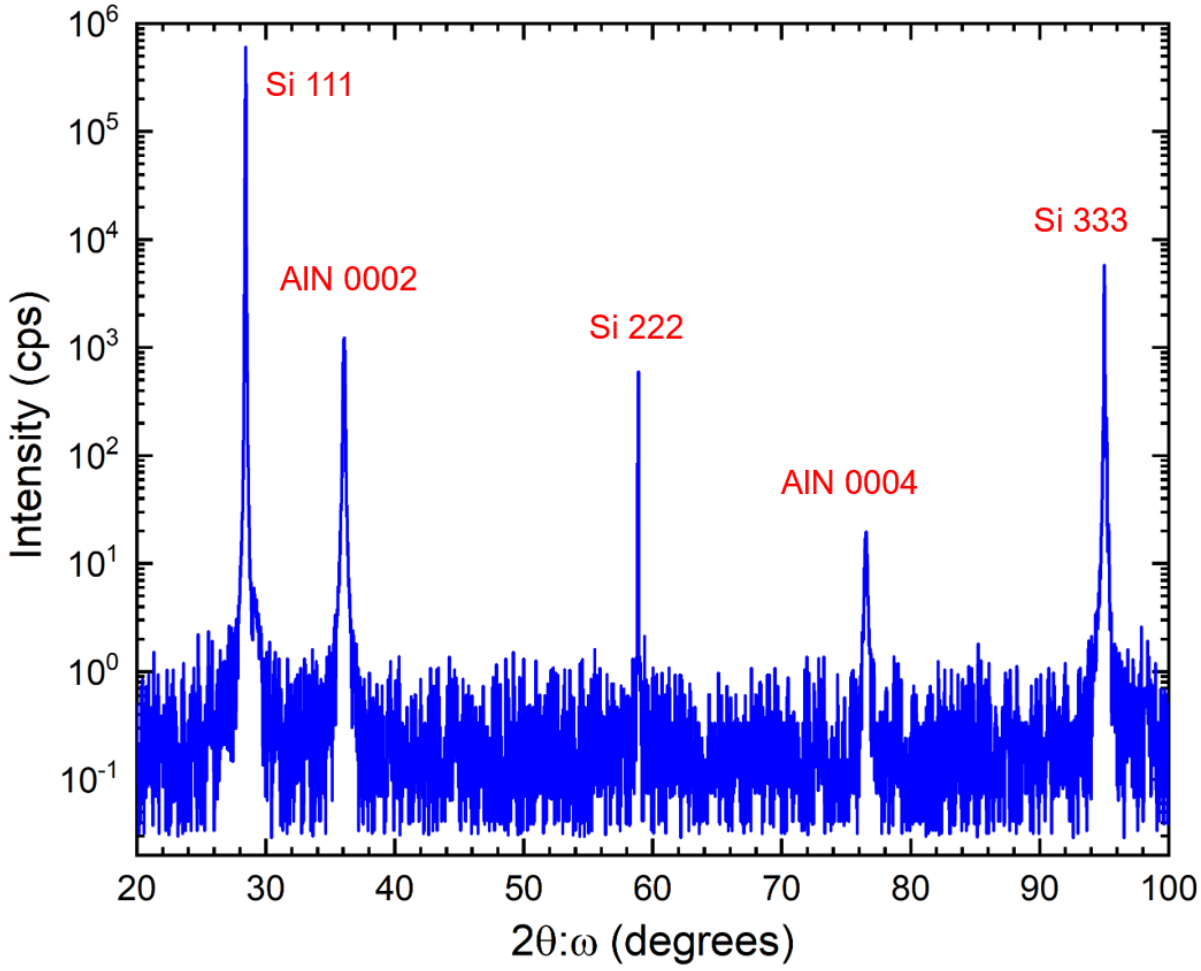

Figure 29: 2ϑ:ω scan for AlN on Si sample done in DAD A4

5 CONCLUSION AND FUTURE WORK

Single crystal AlN (0001) oriented thin-films grown on Si (111) substrates have been characterized using various XRD techniques, specifically using high-resolution diffraction. Samples with various thicknesses of thin-films have been characterized for film quality and strain. Roughness, density, and thickness measurements from XRR were performed on samples with AlN on Si. The GaN nanowire layer grown on the Si substrate is an effective template for growing high-quality and low-strain AlN thin-films.

AlN grown in the GaN nanowire template is virtually strain free. The strain ranges from 0% to 0.3% in-plane and 0 to 0.04% out-of-plane. The sample grown without the GaN interlayer was slightly higher in strain with 1% in-plane. The FWHM also concurs with GaN interlayer strain results, reducing the FWHM significantly. The RSMs for all the samples indicate broadening in the ω-direction, suggesting out-of-plane tilt in the samples.

For future work, the electrical properties of these samples need to be studied. An optimum thickness for best device performance is to be investigated, and subsequent samples should be prepared. The interface of the samples can be studied using microscopy techniques like TEM to visually see any defects that might be present and further improve the fabrication process. Studies using AlN itself as an electronic material need to be performed rather than just using it as a buffer layer for GaN growth.

REFERENCES

[1] N. E. Christensen and I. Gorczyca, “Optical and structural properties of III-V nitrides under pressure,” *Phys. Rev. B*, vol. 50, no. 7, pp. 4397–4415, Aug. 1994, doi: 10.1103/PhysRevB.50.4397.

[2] Y. N. Xu and W. Y. Ching, “Electronic, optical, and structural properties of some wurtzite crystals,” *Phys. Rev. B*, vol. 48, no. 7, pp. 4335–4351, 1993, doi: 10.1103/PhysRevB.48.4335.

[3] X. Yin, Q. Zhang, and S. Zhao, “Molecular Beam Epitaxial Growth of AlN Thin Films on Si through Exploiting Low Al Adatom Migration and the Nitrogen-Rich Environment on a Nanowire Template,” *Cryst. Growth Des.*, vol. 21, no. 7, pp. 3645–3649, Jul. 2021, doi: 10.1021/acs.cgd.1c00327.

[4] J. C. Zhang *et al.*, “The influence of AlN buffer layer thickness on the properties of GaN epilayer,” *J. Cryst. Growth*, vol. 268, no. 1–2, pp. 24–29, 2004, doi: 10.1016/j.jcrysgro.2004.04.102.

[5] Y. Huttel, H. Gomez, A. Cebollada, G. Armelles, and M. I. Alonso, “Epitaxial growth of AlN on sapphire (0001) by sputtering: a structural, morphological and optical study,” *J. Cryst. Growth*, vol. 242, no. 1, pp. 116–123, 2002, doi: https://doi.org/10.1016/S0022-0248(02)01375-1.

[6] K.-H. "Kim, Y.-S. "Kim, S.-H. "Jeong, S.-W. [Cheongju U. “Jung Chungbuk (Korea, Republic of)],” and S.-H. [Sejong U. “Lee Seoul (Korea, Republic of)],” “Fabrication and properties of an epitaxial AlN film on a SiC substrate by using reactive RF magnetron sputtering,” vol. 48, 2006, doi: https://doi.org/.

[7] G. F. Harrington *et al.*, “Synthesis of c-axis oriented AlN thin films on different substrates: A review,” *Semicond. Sci. Technol.*, vol. 184, no. 7, pp. 4724–4728, 2021, doi: 10.1021/acs.cgd.1c00327.

[8] S. Nakanishi and T. Horiguchi, “Surface Lattice Constants of Si (111), Ni (111) and,” *Jpn. J. Appl. Phys.*, vol. 20, no. 111, pp. 214–216, 1981, [Online]. Available: https://iopscience.iop.org/article/10.1143/JJAP.20.L214/meta.

[9] G. F. Harrington and J. Santiso, “Back-to-Basics tutorial: X-ray diffraction of thin films,” *J. Electroceramics*, vol. 47, no. 4, pp. 141–163, 2021, doi: 10.1007/s10832-021-00263-6.

[10] M. Sardela, *Practical materials characterization*. 2014.

[11] G. Bracco and B. Holst, “Surface science techniques,” *Springer Ser. Surf. Sci.*, vol. 51, no. 1, 2013, doi: 10.1007/978-3-642-34243-1.

[12] M. Wormington, D. K. Bowen, and B. K. Tanner, “Principles and Performance of a PC-Based Program for Simulation of Grazing Incidence X-Ray Reflectivity Profiles,” *MRS Proc.*, vol. 238, p. 119, 1991, doi: DOI: 10.1557/PROC-238-119.

[13] E. H. Chason and T. Mayer, “Thin film and surface characterization by specular X-ray reflectivity,” *Crit. Rev. Solid State Mater. Sci.*, vol. 22, pp. 1–67, 1997, [Online]. Available: https://api.semanticscholar.org/CorpusID:93330011.

[14] B. R. Yeom, R. Navamathavan, J. H. Park, Y. H. Ra, and C. R. Lee, “Growth behavior of GaN epilayers on Si(111) grown by GaN nanowires assisted epitaxial lateral overgrowth,” *CrystEngComm*, vol. 14, no. 17, pp. 5558–5563, 2012, doi: 10.1039/c2ce25142f.

[15] M. E. Liao, “Cadmium Telluride and Grain Boundaries: A Preliminary Study,” University of California, Los Angeles PP - United States -- California, United States -- California, 2017.

[16] D. Windover, D. L. Gil, A. Henins, and J. P. Cline, “NIST High Resolution X-Ray Diffraction Standard Reference Material: SRM 2000,” *AIP Conf. Proc.*, vol. 1173, no. 1, pp. 50–54, Sep. 2009, doi: 10.1063/1.3251259.

[17] Y. Feng *et al.*, “Competitive growth mechanisms of AlN on Si (111) by MOVPE,” *Sci. Rep.*, vol. 3, Sep. 2014, doi: 10.1038/srep06416.

[18] D. K. Bowen and B. K. Tanner, *High resolution X-ray diffractometry and topography*. 1998.

[19] D. Litvinov, D. Gerthsen, R. Vöhringer, D. Z. Hu, and D. M. Schaadt, “Transmission electron microscopy investigation of AlN growth on Si(111),” *J. Cryst. Growth*, vol. 338, no. 1, pp. 283–290, 2012, doi: 10.1016/j.jcrysgro.2011.11.038.

[20] P. Zaumseil, “High-resolution characterization of the forbidden Si 200 and Si 222 reflections,” *J. Appl. Crystallogr.*, vol. 48, pp. 528–532, 2015, doi: 10.1107/S1600576715004732.